

# Measurements of the Lineshape of the $Z^0$ and Determination of Electroweak Parameters from its Hadronic and Leptonic Decays

DELPHI Collaboration

## Abstract

During the LEP running periods in 1990 and 1991 DELPHI has accumulated approximately 450,000  $Z^0$  decays into hadrons and charged leptons. The increased event statistics coupled with improved analysis techniques and improved knowledge of the LEP beam energies permit significantly better measurements of the mass and width of the  $Z^0$  resonance. Model independent fits to the cross sections and leptonic forward-backward asymmetries yield the following  $Z^0$  parameters: the mass and total width  $M_Z = 91.187 \pm 0.009$  GeV,  $\Gamma_Z = 2.486 \pm 0.012$  GeV, the hadronic and leptonic partial widths  $\Gamma_{\text{had}} = 1.725 \pm 0.012$  GeV,  $\Gamma_l = 83.01 \pm 0.52$  MeV, the invisible width  $\Gamma_{\text{inv}} = 512 \pm 10$  MeV, the ratio of hadronic to leptonic partial widths  $R_l = 20.78 \pm 0.15$ , and the Born level hadronic peak cross section  $\sigma_0 = 40.90 \pm 0.28$  nb. Using these results and the value of  $\alpha_s$  determined from DELPHI data, the number of light neutrino species is determined to be  $3.08 \pm 0.05$ . The individual leptonic widths are found to be:  $\Gamma_e = 82.93 \pm 0.70$  MeV,  $\Gamma_\mu = 83.20 \pm 1.11$  MeV and  $\Gamma_\tau = 82.89 \pm 1.31$  MeV. Using the measured leptonic forward-backward asymmetries and assuming lepton universality, the squared vector and axial-vector couplings of the  $Z^0$  to charged leptons are found to be  $g_{V_l}^2 = (1.47 \pm 0.51) \times 10^{-3}$  and  $g_{A_l}^2 = 0.2483 \pm 0.0016$ . A full Standard Model fit to the data yields a value of the top mass  $m_t = 115_{-82}^{+52}(\text{expt.})_{-24}^{+23}(\text{Higgs})$  GeV, corresponding to a value of the weak mixing angle  $\sin^2\theta_{\text{eff}}^{\text{lept}} = 0.2339 \pm 0.0015(\text{expt.})_{-0.0004}^{+0.0001}(\text{Higgs})$ . Values are obtained for the variables S and T, or  $\epsilon_1$  and  $\epsilon_3$  which parameterize electroweak loop effects.

(To be submitted to Nuclear Physics B)

P.Abreu<sup>20</sup>, W.Adam<sup>7</sup>, T.Adye<sup>37</sup>, E.Agasi<sup>30</sup>, R.Aleksan<sup>39</sup>, G.D.Alekseev<sup>14</sup>, A.Algeri<sup>13</sup>, P.Allport<sup>21</sup>,  
 S.Almehed<sup>23</sup>, F.M.L.Almeida Junior<sup>48</sup>, S.J.Alvsvaag<sup>4</sup>, U.Amaldi<sup>7</sup>, A.Andreazza<sup>27</sup>, P.Antilogus<sup>24</sup>, W-D.Apel<sup>15</sup>,  
 R.J.Apsimon<sup>37</sup>, Y.Arnaud<sup>39</sup>, B.Åsman<sup>45</sup>, J-E.Augustin<sup>18</sup>, A.Augustinus<sup>30</sup>, P.Baillon<sup>7</sup>, P.Bambade<sup>18</sup>, F.Barao<sup>20</sup>,  
 R.Barate<sup>12</sup>, G.Barbiellini<sup>47</sup>, D.Y.Bardin<sup>14</sup>, G.J.Barker<sup>34</sup>, A.Baroncelli<sup>41</sup>, O.Barring<sup>7</sup>, J.A.Barrio<sup>25</sup>, W.Bartl<sup>51</sup>,  
 M.J.Bates<sup>37</sup>, M.Battaglia<sup>13</sup>, M.Baubillier<sup>22</sup>, K-H.Becks<sup>53</sup>, M.Begalli<sup>36</sup>, P.Beilliere<sup>6</sup>, Yu.Belokopytov<sup>43</sup>,  
 P.Beltran<sup>9</sup>, A.C.Benvenuti<sup>5</sup>, M.Berggren<sup>18</sup>, D.Bertrand<sup>2</sup>, F.Bianchi<sup>46</sup>, M.Bigi<sup>46</sup>, M.S.Bilenky<sup>14</sup>, P.Billoir<sup>22</sup>,  
 J.Bjarne<sup>23</sup>, D.Bloch<sup>8</sup>, J.Blocki<sup>52</sup>, S.Blyth<sup>34</sup>, V.Bocci<sup>38</sup>, P.N.Bogolubov<sup>14</sup>, T.Bolognese<sup>39</sup>, M.Bonesini<sup>27</sup>,  
 W.Bonivento<sup>27</sup>, P.S.L.Booth<sup>21</sup>, G.Borisov<sup>43</sup>, C.Bosio<sup>41</sup>, B.Bostjancic<sup>44</sup>, S.Bosworth<sup>34</sup>, O.Botner<sup>49</sup>,  
 E.Boudinov<sup>43</sup>, B.Bouquet<sup>18</sup>, C.Bourdarios<sup>18</sup>, T.J.V.Bowcock<sup>21</sup>, M.Bozzo<sup>11</sup>, S.Braibant<sup>2</sup>, P.Branchini<sup>41</sup>,  
 K.D.Brand<sup>35</sup>, R.A.Brenner<sup>13</sup>, H.Briand<sup>22</sup>, C.Bricman<sup>2</sup>, L.Brillault<sup>22</sup>, R.C.A.Brown<sup>7</sup>, P.Bruckman<sup>16</sup>,  
 J-M.Brunet<sup>6</sup>, A.Budziak<sup>16</sup>, L.Bugge<sup>32</sup>, T.Buran<sup>32</sup>, A.Buys<sup>7</sup>, J.A.M.A.Buytaert<sup>7</sup>, M.Caccia<sup>27</sup>, M.Calvi<sup>27</sup>,  
 A.J.Camacho Rozas<sup>42</sup>, R.Campion<sup>21</sup>, T.Camporesi<sup>7</sup>, V.Canale<sup>38</sup>, K.Cankocak<sup>45</sup>, F.Cao<sup>2</sup>, F.Carena<sup>7</sup>,  
 P.Carrilho<sup>48</sup>, L.Carroll<sup>21</sup>, C.Caso<sup>11</sup>, M.V.Castillo Gimenez<sup>50</sup>, A.Cattai<sup>7</sup>, F.R.Cavallo<sup>5</sup>, L.Cerrito<sup>38</sup>,  
 V.Chabaud<sup>7</sup>, A.Chan<sup>1</sup>, Ph.Charpentier<sup>7</sup>, J.Chauveau<sup>22</sup>, P.Checchia<sup>35</sup>, G.A.Chelkov<sup>14</sup>, L.Chevalier<sup>39</sup>,  
 P.Chliapnikov<sup>43</sup>, V.Chorowicz<sup>22</sup>, J.T.M.Chrin<sup>50</sup>, V.Cindro<sup>44</sup>, P.Collins<sup>34</sup>, J.L.Contreras<sup>18</sup>, R.Contri<sup>11</sup>,  
 E.Cortina<sup>50</sup>, G.Cosme<sup>18</sup>, F.Couchot<sup>18</sup>, H.B.Crawley<sup>1</sup>, D.Crennell<sup>37</sup>, G.Crosetti<sup>11</sup>, J.Cuevas Maestro<sup>33</sup>,  
 S.Czellar<sup>13</sup>, E.Dahl-Jensen<sup>28</sup>, J.Dahm<sup>53</sup>, B.Dalmagne<sup>18</sup>, M.Dam<sup>32</sup>, G.Damgaard<sup>28</sup>, E.Daubie<sup>2</sup>, A.Daum<sup>15</sup>,  
 P.D.Dauncey<sup>7</sup>, M.Davenport<sup>7</sup>, J.Davies<sup>21</sup>, W.Da Silva<sup>22</sup>, C.Defoix<sup>6</sup>, P.Delpierre<sup>26</sup>, N.Demaria<sup>46</sup>,  
 A.De Angelis<sup>7</sup>, H.De Boeck<sup>2</sup>, W.De Boer<sup>15</sup>, S.De Brabandere<sup>2</sup>, C.De Clercq<sup>2</sup>, M.D.M.De Fez Laso<sup>50</sup>,  
 C.De La Vaissiere<sup>22</sup>, B.De Lotto<sup>47</sup>, A.De Min<sup>27</sup>, L.De Paula<sup>48</sup>, H.Dijkstra<sup>7</sup>, L.Di Ciaccio<sup>38</sup>, F.Djama<sup>8</sup>,  
 J.Dolbeau<sup>6</sup>, M.Donszelmann<sup>7</sup>, K.Doroba<sup>52</sup>, M.Dracos<sup>8</sup>, J.Drees<sup>53</sup>, M.Dris<sup>31</sup>, Y.Dufour<sup>7</sup>, F.Dupont<sup>12</sup>, D.Edsall<sup>1</sup>,  
 L-O.Eek<sup>49</sup>, R.Ehret<sup>15</sup>, T.Ekelof<sup>49</sup>, G.Ekspong<sup>45</sup>, A.Elliot Peisert<sup>7</sup>, M.Elsing<sup>53</sup>, J-P.Engel<sup>8</sup>, N.Ershaidat<sup>22</sup>,  
 M.Espirito Santo<sup>20</sup>, V.Falaleev<sup>43</sup>, D.Fassouliotis<sup>31</sup>, M.Feindt<sup>7</sup>, A.Ferrer<sup>50</sup>, T.A.Filippas<sup>31</sup>, A.Firestone<sup>1</sup>,  
 H.Foeth<sup>7</sup>, E.Fokitis<sup>31</sup>, F.Fontanelli<sup>11</sup>, K.A.J.Forbes<sup>21</sup>, J-L.Fousset<sup>26</sup>, S.Francon<sup>24</sup>, B.Franek<sup>37</sup>, P.Frenkiel<sup>6</sup>,  
 D.C.Fries<sup>15</sup>, A.G.Frodesen<sup>4</sup>, R.Fruhworth<sup>51</sup>, F.Fulda-Quenzer<sup>18</sup>, H.Furstenau<sup>7</sup>, J.Fuster<sup>7</sup>, D.Gamba<sup>46</sup>,  
 M.Gandelman<sup>17</sup>, C.Garcia<sup>50</sup>, J.Garcia<sup>42</sup>, C.Gaspar<sup>7</sup>, U.Gasparini<sup>35</sup>, Ph.Gavillet<sup>7</sup>, E.N.Gaziz<sup>31</sup>, J-P.Gerber<sup>8</sup>,  
 P.Giacomelli<sup>7</sup>, D.Gillespie<sup>7</sup>, R.Gokiel<sup>52</sup>, B.Golob<sup>44</sup>, V.M.Golovatyuk<sup>14</sup>, J.J.Gomez Y Cadenas<sup>7</sup>, G.Gopal<sup>37</sup>,  
 L.Gorn<sup>1</sup>, M.Gorski<sup>52</sup>, V.Gracco<sup>11</sup>, F.Grad<sup>2</sup>, E.Graziani<sup>41</sup>, G.Grosdidier<sup>18</sup>, B.Grossetete<sup>22</sup>, P.Gunnarsson<sup>45</sup>,  
 J.Guy<sup>37</sup>, U.Haeding<sup>15</sup>, F.Hahn<sup>53</sup>, M.Hahn<sup>45</sup>, S.Hahn<sup>53</sup>, S.Haider<sup>30</sup>, Z.Hajduk<sup>16</sup>, A.Hakansson<sup>23</sup>,  
 A.Hallgren<sup>49</sup>, K.Hamacher<sup>53</sup>, G.Hamel De Monchenault<sup>39</sup>, W.Hao<sup>30</sup>, F.J.Harris<sup>34</sup>, V.Hedberg<sup>23</sup>, R.Henriques<sup>20</sup>,  
 J.J.Hernandez<sup>50</sup>, J.A.Hernando<sup>50</sup>, P.Herquet<sup>2</sup>, H.Herr<sup>7</sup>, T.L.Hessing<sup>21</sup>, I.Hietanen<sup>13</sup>, C.O.Higgins<sup>21</sup>, E.Higon<sup>50</sup>,  
 H.J.Hilke<sup>7</sup>, T.S.Hill<sup>1</sup>, S.D.Hodgson<sup>34</sup>, T.Hofmohl<sup>52</sup>, S-O.Holmgren<sup>45</sup>, P.J.Holt<sup>34</sup>, D.Holthuizen<sup>30</sup>, P.F.Honore<sup>6</sup>,  
 M.Houlden<sup>21</sup>, J.Hrubic<sup>51</sup>, K.Huet<sup>2</sup>, K.Hultqvist<sup>45</sup>, P.Ioannou<sup>3</sup>, P-S.Iversen<sup>4</sup>, J.N.Jackson<sup>21</sup>, R.Jacobsson<sup>45</sup>,  
 P.Jalocha<sup>16</sup>, G.Jarlskog<sup>23</sup>, P.Jarry<sup>39</sup>, B.Jean-Marie<sup>18</sup>, E.K.Johansson<sup>45</sup>, M.Jonker<sup>7</sup>, L.Jonsson<sup>23</sup>, P.Juillot<sup>8</sup>,  
 G.Kalkanis<sup>3</sup>, G.Kalmus<sup>37</sup>, F.Kapusta<sup>22</sup>, M.Karlsson<sup>45</sup>, E.Karvelas<sup>9</sup>, S.Katsanevas<sup>3</sup>, E.C.Katsoufis<sup>31</sup>,  
 R.Keranen<sup>7</sup>, B.A.Khomenko<sup>14</sup>, N.N.Khovanski<sup>14</sup>, B.King<sup>21</sup>, N.J.Kjaer<sup>28</sup>, H.Klein<sup>7</sup>, A.Klovning<sup>4</sup>, P.Kluit<sup>30</sup>,  
 A.Koch-Mehrin<sup>53</sup>, J.H.Koehne<sup>15</sup>, B.Koene<sup>30</sup>, P.Kokkinias<sup>9</sup>, M.Koratzinos<sup>32</sup>, A.V.Korytov<sup>14</sup>, V.Kostioukhine<sup>43</sup>,  
 C.Kourkoumelis<sup>3</sup>, O.Kouznetsov<sup>14</sup>, P.H.Kramer<sup>53</sup>, M.Krammer<sup>51</sup>, C.Kreuter<sup>15</sup>, J.Krolkowski<sup>52</sup>, I.Kronkvist<sup>23</sup>,  
 W.Kucewicz<sup>16</sup>, K.Kulka<sup>49</sup>, K.Kurvinen<sup>13</sup>, C.Lacasta<sup>50</sup>, C.Lambropoulos<sup>9</sup>, J.W.Lamsa<sup>1</sup>, L.Lanceri<sup>47</sup>,  
 P.Langefeld<sup>53</sup>, V.Lapin<sup>43</sup>, I.Last<sup>21</sup>, J-P.Laugier<sup>39</sup>, R.Lauhakangas<sup>13</sup>, G.Leder<sup>51</sup>, F.Ledroit<sup>12</sup>, R.Leitner<sup>29</sup>,  
 Y.Lemoigne<sup>39</sup>, J.Lemonne<sup>2</sup>, G.Lenzen<sup>53</sup>, V.Lepeltier<sup>18</sup>, J.M.Levy<sup>8</sup>, E.Lieb<sup>53</sup>, J.Lindgren<sup>13</sup>, R.Lindner<sup>53</sup>,  
 A.Lipniacka<sup>18</sup>, I.Lippi<sup>35</sup>, B.Loerstad<sup>23</sup>, M.Lokajicek<sup>10</sup>, J.G.Loken<sup>34</sup>, A.Lopez-Fernandez<sup>7</sup>, M.A.Lopez Aguera<sup>42</sup>,  
 M.Los<sup>30</sup>, D.Loukas<sup>9</sup>, J.J.Lozano<sup>50</sup>, P.Lutz<sup>6</sup>, L.Lyons<sup>34</sup>, G.Maehlum<sup>32</sup>, J.Maillard<sup>6</sup>, A.Maio<sup>20</sup>, A.Maltezos<sup>9</sup>,  
 F.Mandl<sup>51</sup>, J.Marco<sup>42</sup>, B.Marechal<sup>48</sup>, M.Margoni<sup>35</sup>, J-C.Marin<sup>7</sup>, C.Mariotti<sup>41</sup>, A.Markou<sup>9</sup>, T.Maron<sup>53</sup>,  
 S.Marti<sup>50</sup>, C.Martinez-Rivero<sup>42</sup>, F.Martinez-Vidal<sup>50</sup>, F.Matorras<sup>42</sup>, C.Matteuzzi<sup>27</sup>, G.Matthiae<sup>38</sup>,  
 M.Mazzucato<sup>35</sup>, M.Mc Cubbin<sup>21</sup>, R.Mc Kay<sup>1</sup>, R.Mc Nulty<sup>21</sup>, J.Medbo<sup>49</sup>, C.Meroni<sup>27</sup>, W.T.Meyer<sup>1</sup>,  
 M.Michelotto<sup>35</sup>, I.Mikulec<sup>51</sup>, L.Mirabito<sup>24</sup>, W.A.Mitaroff<sup>51</sup>, G.V.Mitselmakher<sup>14</sup>, U.Mjoernmark<sup>23</sup>, T.Moa<sup>45</sup>,  
 R.Moeller<sup>28</sup>, K.Moenig<sup>7</sup>, M.R.Monge<sup>11</sup>, P.Morettini<sup>11</sup>, H.Mueller<sup>15</sup>, W.J.Murray<sup>37</sup>, B.Muryn<sup>16</sup>, G.Myatt<sup>34</sup>,  
 F.Naraghi<sup>12</sup>, F.L.Navarría<sup>5</sup>, P.Negri<sup>27</sup>, S.Nemecsek<sup>10</sup>, W.Neumann<sup>53</sup>, N.Neumeister<sup>51</sup>, R.Nicolaidou<sup>3</sup>,  
 B.S.Nielsen<sup>28</sup>, V.Nikolaenko<sup>43</sup>, P.E.S.Nilsen<sup>4</sup>, P.Niss<sup>45</sup>, A.Nomerotski<sup>35</sup>, V.Obraztsov<sup>43</sup>, A.G.Olshevski<sup>14</sup>,  
 R.Orava<sup>13</sup>, A.Ostankov<sup>43</sup>, K.Osterberg<sup>13</sup>, A.Ouraou<sup>39</sup>, P.Paganini<sup>18</sup>, M.Paganoni<sup>27</sup>, R.Pain<sup>22</sup>, H.Palka<sup>16</sup>,  
 Th.D.Papadopoulou<sup>31</sup>, L.Pape<sup>7</sup>, F.Parodi<sup>11</sup>, A.Passeri<sup>41</sup>, M.Pegoraro<sup>35</sup>, J.Pennanen<sup>13</sup>, L.Peralta<sup>20</sup>,  
 H.Pernegger<sup>51</sup>, M.Pernicka<sup>51</sup>, A.Perrotta<sup>5</sup>, C.Petridou<sup>47</sup>, A.Petrolini<sup>11</sup>, G.Piana<sup>11</sup>, F.Pierre<sup>39</sup>, M.Pimenta<sup>20</sup>,  
 S.Plaszczynski<sup>18</sup>, O.Podobrin<sup>15</sup>, M.E.Pol<sup>17</sup>, G.Polok<sup>16</sup>, P.Poropat<sup>47</sup>, V.Pozdniakov<sup>14</sup>, M.Prest<sup>47</sup>, P.Privitera<sup>38</sup>,  
 A.Pullia<sup>27</sup>, D.Radojicic<sup>34</sup>, S.Ragazzi<sup>27</sup>, H.Rahmani<sup>31</sup>, J.Rames<sup>10</sup>, P.N.Ratoff<sup>19</sup>, A.L.Read<sup>32</sup>, M.Reale<sup>53</sup>,  
 P.Rebecchi<sup>18</sup>, N.G.Redaeli<sup>27</sup>, M.Regler<sup>51</sup>, D.Reid<sup>7</sup>, P.B.Renton<sup>34</sup>, L.K.Resvanis<sup>3</sup>, F.Richard<sup>18</sup>, J.Richardson<sup>21</sup>,  
 J.Ridky<sup>10</sup>, G.Rinaudo<sup>46</sup>, A.Romero<sup>46</sup>, I.Roncagliolo<sup>11</sup>, P.Ronchese<sup>35</sup>, C.Ronnqvist<sup>13</sup>, E.I.Rosenberg<sup>1</sup>, E.Rosso<sup>7</sup>,  
 P.Roudeau<sup>18</sup>, T.Rovelli<sup>5</sup>, W.Ruckstuhl<sup>30</sup>, V.Ruhlmann-Kleider<sup>39</sup>, A.Ruiz<sup>42</sup>, K.Rybicki<sup>16</sup>, H.Saarikko<sup>13</sup>,

Y.Sacquin<sup>39</sup>, G.Sajot<sup>12</sup>, J.Salt<sup>50</sup>, J.Sanchez<sup>25</sup>, M.Sannino<sup>11,40</sup>, S.Schael<sup>7</sup>, H.Schneider<sup>15</sup>, M.A.E.Schyns<sup>53</sup>, G.Sciolla<sup>46</sup>, F.Scuri<sup>47</sup>, A.M.Segar<sup>34</sup>, A.Seitz<sup>15</sup>, R.Sekulin<sup>37</sup>, M.Sessa<sup>47</sup>, R.Seufert<sup>15</sup>, R.C.Shellard<sup>36</sup>, I.Siccama<sup>30</sup>, P.Siegrist<sup>39</sup>, S.Simonetti<sup>11</sup>, F.Simonetto<sup>35</sup>, A.N.Sisakian<sup>14</sup>, G.Skjevling<sup>32</sup>, G.Smadja<sup>39,24</sup>, N.Smirnov<sup>43</sup>, O.Smirnova<sup>14</sup>, G.R.Smith<sup>37</sup>, R.Sosnowski<sup>52</sup>, D.Souza-Santos<sup>36</sup>, T.Spaso<sup>20</sup>, E.Spiriti<sup>41</sup>, S.Squarcia<sup>11</sup>, H.Staek<sup>53</sup>, C.Stanescu<sup>41</sup>, S.Stapnes<sup>32</sup>, G.Stavropoulos<sup>9</sup>, F.Stichelbaut<sup>7</sup>, A.Stocchi<sup>18</sup>, J.Strauss<sup>51</sup>, J.Straver<sup>7</sup>, R.Strub<sup>8</sup>, B.Stugu<sup>4</sup>, M.Szczekowski<sup>52</sup>, M.Szeptycka<sup>52</sup>, P.Szymanski<sup>52</sup>, T.Tabarelli<sup>27</sup>, O.Tchikilev<sup>43</sup>, G.E.Theodosiou<sup>9</sup>, Z.Thome<sup>48</sup>, A.Tilquin<sup>26</sup>, J.Timmermans<sup>30</sup>, V.G.Timofeev<sup>14</sup>, L.G.Tkatchev<sup>14</sup>, T.Todorov<sup>8</sup>, D.Z.Toet<sup>30</sup>, O.Toker<sup>13</sup>, A.Tomaradze<sup>2</sup>, B.Tome<sup>20</sup>, E.Torassa<sup>46</sup>, L.Tortora<sup>41</sup>, D.Treille<sup>7</sup>, W.Trischuk<sup>7</sup>, G.Tristram<sup>6</sup>, C.Troncon<sup>27</sup>, A.Tsirou<sup>7</sup>, E.N.Tsyganov<sup>14</sup>, M.Turala<sup>16</sup>, M-L.Turluer<sup>39</sup>, T.Tuuva<sup>13</sup>, I.A.Tyapkin<sup>22</sup>, M.Tyndel<sup>37</sup>, S.Tzamaras<sup>21</sup>, B.Ueberschaer<sup>53</sup>, S.Ueberschaer<sup>53</sup>, O.Ullaland<sup>7</sup>, V.Uvarov<sup>43</sup>, G.Valenti<sup>5</sup>, E.Vallazza<sup>7</sup>, J.A.Valls Ferrer<sup>50</sup>, C.Vander Velde<sup>2</sup>, G.W.Van Apeldoorn<sup>30</sup>, P.Van Dam<sup>30</sup>, M.Van Der Heijden<sup>30</sup>, W.K.Van Doninck<sup>2</sup>, J.Van Eldik<sup>30</sup>, P.Vaz<sup>7</sup>, G.Vegni<sup>27</sup>, L.Ventura<sup>35</sup>, W.Venus<sup>37</sup>, F.Verbeure<sup>2</sup>, M.Verlato<sup>35</sup>, L.S.Vertogradov<sup>14</sup>, D.Vilanova<sup>39</sup>, P.Vincent<sup>24</sup>, L.Vitale<sup>47</sup>, E.Vlasov<sup>43</sup>, A.S.Vodopyanov<sup>14</sup>, M.Vollmer<sup>53</sup>, M.Voutilainen<sup>13</sup>, V.Vrba<sup>10</sup>, H.Wahlen<sup>53</sup>, C.Walck<sup>45</sup>, F.Waldner<sup>47</sup>, A.Wehr<sup>53</sup>, M.Weierstall<sup>53</sup>, P.Weilhammer<sup>7</sup>, A.M.Wetherell<sup>7</sup>, J.H.Wickens<sup>2</sup>, M.Wielers<sup>15</sup>, G.R.Wilkinson<sup>34</sup>, W.S.C.Williams<sup>34</sup>, M.Winter<sup>8</sup>, G.Wormser<sup>18</sup>, K.Woschnagg<sup>49</sup>, A.Zaitsev<sup>43</sup>, A.Zalewska<sup>16</sup>, L.Zanini<sup>46</sup>, D.Zavrtanik<sup>44</sup>, E.Zevgolatakos<sup>9</sup>, N.I.Zimin<sup>14</sup>, M.Zito<sup>39</sup>, D.Zontar<sup>44</sup>, R.Zuberi<sup>34</sup>, G.Zumerle<sup>35</sup>, J.Zuniga<sup>50</sup>

<sup>1</sup> Ames Laboratory and Department of Physics, Iowa State University, Ames IA 50011, USA

<sup>2</sup> Physics Department, Univ. Instelling Antwerpen, Universiteitsplein 1, B-2610 Wilrijk, Belgium

and IIHE, ULB-VUB, Pleinlaan 2, B-1050 Brussels, Belgium

and Faculté des Sciences, Univ. de l'Etat Mons, Av. Maistriau 19, B-7000 Mons, Belgium

<sup>3</sup> Physics Laboratory, University of Athens, Solonos Str. 104, GR-10680 Athens, Greece

<sup>4</sup> Department of Physics, University of Bergen, Allégaten 55, N-5007 Bergen, Norway

<sup>5</sup> Dipartimento di Fisica, Università di Bologna and INFN, Via Irnerio 46, I-40126 Bologna, Italy

<sup>6</sup> Collège de France, Lab. de Physique Corpusculaire, IN2P3-CNRS, F-75231 Paris Cedex 05, France

<sup>7</sup> CERN, CH-1211 Geneva 23, Switzerland

<sup>8</sup> Centre de Recherche Nucléaire, IN2P3 - CNRS/ULP - BP20, F-67037 Strasbourg Cedex, France

<sup>9</sup> Institute of Nuclear Physics, N.C.S.R. Demokritos, P.O. Box 60228, GR-15310 Athens, Greece

<sup>10</sup> FZU, Inst. of Physics of the C.A.S. High Energy Physics Division, Na Slovance 2, CS-180 40, Praha 8, Czechoslovakia

<sup>11</sup> Dipartimento di Fisica, Università di Genova and INFN, Via Dodecaneso 33, I-16146 Genova, Italy

<sup>12</sup> Institut des Sciences Nucléaires, IN2P3-CNRS, Université de Grenoble 1, F-38026 Grenoble, France

<sup>13</sup> Research Institute for High Energy Physics, SEFT, P.O. Box 9, FIN-00014 University of Helsinki, Finland

<sup>14</sup> Joint Institute for Nuclear Research, Dubna, Head Post Office, P.O. Box 79, 101 000 Moscow, Russian Federation

<sup>15</sup> Institut für Experimentelle Kernphysik, Universität Karlsruhe, Postfach 6980, D-76128 Karlsruhe, Germany

<sup>16</sup> High Energy Physics Laboratory, Institute of Nuclear Physics, Ul. Kawiory 26a, PL-30055 Krakow 30, Poland

<sup>17</sup> Centro Brasileiro de Pesquisas Físicas, rua Xavier Sigaud 150, RJ-22290 Rio de Janeiro, Brazil

<sup>18</sup> Université de Paris-Sud, Lab. de l'Accélérateur Linéaire, IN2P3-CNRS, Bat 200, F-91405 Orsay, France

<sup>19</sup> School of Physics and Materials, University of Lancaster, GB-Lancaster LA1 4YB, UK

<sup>20</sup> LIP, IST, FCUL - Av. Elias Garcia, 14-1º, P-1000 Lisboa Codex, Portugal

<sup>21</sup> Department of Physics, University of Liverpool, P.O. Box 147, GB-Liverpool L69 3BX, UK

<sup>22</sup> LPNHE, IN2P3-CNRS, Universités Paris VI et VII, Tour 33 (RdC), 4 place Jussieu, F-75252 Paris Cedex 05, France

<sup>23</sup> Department of Physics, University of Lund, Sölvegatan 14, S-22363 Lund, Sweden

<sup>24</sup> Université Claude Bernard de Lyon, IPNL, IN2P3-CNRS, F-69622 Villeurbanne Cedex, France

<sup>25</sup> Universidad Complutense, Avda. Complutense s/n, E-28040 Madrid, Spain

<sup>26</sup> Univ. d'Aix - Marseille II - CPP, IN2P3-CNRS, F-13288 Marseille Cedex 09, France

<sup>27</sup> Dipartimento di Fisica, Università di Milano and INFN, Via Celoria 16, I-20133 Milan, Italy

<sup>28</sup> Niels Bohr Institute, Blegdamsvej 17, DK-2100 Copenhagen 0, Denmark

<sup>29</sup> NC, Nuclear Centre of MFF, Charles University, Areal MFF, V Holesovickach 2, CS-180 00, Praha 8, Czechoslovakia

<sup>30</sup> NIKHEF-H, Postbus 41882, NL-1009 DB Amsterdam, The Netherlands

<sup>31</sup> National Technical University, Physics Department, Zografou Campus, GR-15773 Athens, Greece

<sup>32</sup> Physics Department, University of Oslo, Blindern, N-1000 Oslo 3, Norway

<sup>33</sup> Dpto. Fisica, Univ. Oviedo, C/P.Jimenez Casas, S/N-33006 Oviedo, Spain

<sup>34</sup> Department of Physics, University of Oxford, Keble Road, Oxford OX1 3RH, UK

<sup>35</sup> Dipartimento di Fisica, Università di Padova and INFN, Via Marzolo 8, I-35131 Padua, Italy

<sup>36</sup> Depto. de Fisica, Pontificia Univ. Católica, C.P. 38071 RJ-22453 Rio de Janeiro, Brazil

<sup>37</sup> Rutherford Appleton Laboratory, Chilton, GB - Didcot OX11 0QX, UK

<sup>38</sup> Dipartimento di Fisica, Università di Roma II and INFN, Tor Vergata, I-00173 Rome, Italy

<sup>39</sup> Centre d'Etude de Saclay, DSM/DAPNIA, F-91191 Gif-sur-Yvette Cedex, France

<sup>40</sup> Dipartimento di Fisica-Università di Salerno, I-84100 Salerno, Italy

<sup>41</sup> Istituto Superiore di Sanità, Ist. Naz. di Fisica Nucl. (INFN), Viale Regina Elena 299, I-00161 Rome, Italy

<sup>42</sup> C.E.A.F.M., C.S.I.C. - Univ. Cantabria, Avda. los Castros, S/N-39006 Santander, Spain

<sup>43</sup> Inst. for High Energy Physics, Serpukov P.O. Box 35, Protvino, (Moscow Region), Russian Federation

<sup>44</sup> J. Stefan Institute and Department of Physics, University of Ljubljana, Jamova 39, SI-61000 Ljubljana, Slovenia

<sup>45</sup> Fysikum, Stockholm University, Box 6730, S-113 85 Stockholm, Sweden

<sup>46</sup> Dipartimento di Fisica Sperimentale, Università di Torino and INFN, Via P. Giuria 1, I-10125 Turin, Italy

<sup>47</sup> Dipartimento di Fisica, Università di Trieste and INFN, Via A. Valerio 2, I-34127 Trieste, Italy

and Istituto di Fisica, Università di Udine, I-33100 Udine, Italy

<sup>48</sup> Univ. Federal do Rio de Janeiro, C.P. 68528 Cidade Univ., Ilha do Fundão BR-21945-970 Rio de Janeiro, Brazil

<sup>49</sup> Department of Radiation Sciences, University of Uppsala, P.O. Box 535, S-751 21 Uppsala, Sweden

<sup>50</sup> IFIC, Valencia-CSIC, and D.F.A.M.N., U. de Valencia, Avda. Dr. Moliner 50, E-46100 Burjassot (Valencia), Spain

<sup>51</sup> Institut für Hochenergiephysik, Österr. Akad. d. Wissensch., Nikolsdorfergasse 18, A-1050 Vienna, Austria

<sup>52</sup> Inst. Nuclear Studies and University of Warsaw, Ul. Hoza 69, PL-00681 Warsaw, Poland

<sup>53</sup> Fachbereich Physik, University of Wuppertal, Postfach 100 127, D-5600 Wuppertal 1, Germany

# 1 Introduction

The study of the lineshape of the  $Z^0$  resonance and the analysis of its hadronic and leptonic decays is of primary importance in the determination of the parameters of the electroweak theory. The mass of the  $Z^0$  is a fundamental parameter of the theory. The hadronic and leptonic decay widths, and the leptonic forward-backward asymmetries, are sensitive to the as yet unknown masses of the top quark and Higgs boson. Within the context of the Standard Model, the decay width of the  $Z^0$  into invisible channels allows an accurate determination of the number of light neutrino species. Although previous measurements have ruled out two or four conventional neutrino species, it is nevertheless important to measure the number of neutrino species as accurately as possible in order to limit non-standard models, or conversely, to show evidence for physics beyond the Standard Model.

In ref. [1], measurements of the  $Z^0$  parameters were reported based on an integrated luminosity of approximately  $6.5 \text{ pb}^{-1}$  accumulated by DELPHI during 1989 and 1990. The present paper gives details of the data collected in 1991, corresponding to approximately  $10 \text{ pb}^{-1}$ , taken at 7 different centre-of-mass energies in a scan around the  $Z^0$  peak. Compared to the previously published results, the 1991 data benefitted from smaller statistical and systematic uncertainties. The absolute luminosity was determined, as previously, from the Small Angle Tagger (SAT). However the relative luminosities at the different scan energies were measured by the Very Small Angle Tagger (VSAT), thereby effectively eliminating the statistical errors of the SAT measurement and giving a substantial gain in the overall sensitivity of the measurements. In the light of improved understanding of the SAT monitor, the cross sections of ref. [1] have been re-evaluated with reduced systematic errors. A crucial element of the 1991 scan was the improvement in the understanding of the LEP machine energies as a result of the measurements by the process of resonant depolarization [2].

This paper is organised as follows. In Section 2 some details of the LEP energy determinations are given. Section 3 contains a brief description of the DELPHI detector and trigger system. In Section 4 accounts are given of the absolute luminosity measurement using the SAT, and of the relative luminosity measurements using the VSAT. The selection of hadronic decays and the measurement of the hadronic cross section are described in Section 5. Section 6 contains an account of the selection of leptonic  $Z^0$  decays, the determination of the cross sections and the measurement of forward-backward asymmetries. In Section 7 the results of fits to the data are reported and in Section 8 interpretations within the context of the Standard Model are given. Fits in terms of parameters which are sensitive to physics beyond the Standard Model are presented in Section 9, and Section 10 gives limits on the possible contribution of new particle production to the measured width and invisible width of the  $Z^0$ . Section 11 gives a summary of the results.

## 2 The Energy of the LEP Beams

Resonant depolarization of the electron beam at 46.5 GeV was observed on five separate occasions during the 1991 data-taking period. These results have been published [2]. The temperatures of the LEP magnets were carefully monitored during the depolarization measurements and throughout the scans. For each of the LEP fills an energy is given which takes account of temperature and aging effects and the non-linear response of the LEP magnets. The principal uncertainties are as follows.

- The absolute energy scale is determined with a precision of  $\pm 5.3$  MeV at 93 GeV centre-of-mass energy ( $\sqrt{s}$ ) by resonant depolarization of the electron beam.
- For the other collision energies a local energy scale correction is applied to account for the non-linear response of the dipole magnets. The uncertainty in this correction is fully correlated energy-to-energy, and is up to  $\pm 7.5$  MeV at 88 GeV.
- An uncertainty is included for non-reproducibility. This includes the observed spread of the polarization measurements and uncertainties due to temperature effects and the status of the radiofrequency accelerating cavities. This uncertainty is uncorrelated energy-to-energy and fill-to-fill. It is estimated to be  $\pm 10^{-4}\sqrt{s}$ , and decreases inversely as the square root of the number of fills at a given energy.
- Point-to-point errors are included to allow for higher order terms in the non-linearity correction. These are random energy-to-energy, and amount to  $\pm 3 \cdot 10^{-5}\sqrt{s}$ .
- The energies for the 1990 runs have been re-evaluated using the most recent information. The absolute energy scale of the 1990 data is assigned an uncertainty of  $\pm 26$  MeV.

On 14th August 1991, just before the start of the systematic scan, the energy of the LEP beams showed a step of  $-15$  MeV [3]. Data taken before this time ('pre-scan' points) have therefore a larger energy uncertainty and are treated separately in the fits.

At each energy setting of the LEP machine the collision energies have a spread which can be approximated by a Gaussian of width  $51 \pm 5$  MeV.

In a recent publication [3] the precise LEP energy measurements combined with the data of the LEP collaborations, including some of the data reported in this paper, have been used to determine an accurate value for the Z mass. The result,  $91.187 \pm 0.007$  GeV, includes an uncertainty of  $\pm 6$  MeV coming from the LEP energy measurements.

### 3 The Apparatus and Trigger System

A detailed description of the DELPHI apparatus can be found in ref. [4]. For the present analysis the following parts of the detector are relevant:

- for the measurement of charged particles the Microvertex Detector (VD), the Inner Detector (ID), the Time Projection Chamber (TPC), the Outer Detector(OD) and the Forward Chambers A and B (FCA and FCB);
- for the measurement of electromagnetic energy the High-density Projection Chamber (HPC) and the Forward Electromagnetic Calorimeter (FEMC); these detectors were also used for identifying minimum ionizing particles;
- for the measurement of the hadronic energy and muon identification the Hadron Calorimeter (HCAL), which covered both the barrel and endcap regions;
- for muon identification the barrel (MUB) and endcap (MUF) muon chambers;
- for the trigger, besides the detectors mentioned above, the barrel Time of Flight counters (TOF), the endcap scintillators (HOF) and a scintillator layer embedded in the HPC;
- for the measurement of luminosity (Section 4) the Small Angle Tagger (SAT) and the Very Small Angle Tagger (VSAT).

A major improvement with respect to the 1990 running was the replacement of the two-layer Microvertex Detector in 1991 by one having three layers of silicon strip detectors surrounding a beam pipe of reduced diameter. This detector now has a higher chance of having two or more hits associated to a particle trajectory and this leads to a reduction in the momentum and vertex reconstruction errors in the barrel region [5].

The event trigger for the 1991 data is largely as described in refs. [1] and [4]. However in addition a trigger based on the barrel muon chambers was used. The trigger efficiencies for the hadronic and leptonic events were measured in events taken with redundant trigger combinations. For hadronic events the trigger efficiency was greater than 99.9% over the whole angular range. For  $e^+e^-$  events the efficiency was greater than 99.9% in the polar angle range between  $44^\circ$  and  $136^\circ$ , for  $\mu^+\mu^-$  events  $(99.9 \pm 0.1)\%$  between  $20^\circ$  and  $160^\circ$ , and for  $\tau^+\tau^-$  events  $(99.9 \pm 0.1)\%$  between  $25^\circ$  and  $155^\circ$ .

A right-handed coordinate system is used in this paper. The  $z$ -axis points along the electron beam direction, and the  $y$ -axis is vertical. The polar angle  $\theta$  is measured with respect to the  $z$ -axis, and the azimuthal angle  $\phi$  is measured with respect to the horizontal plane.

## 4 The Luminosity Measurement

This section summarizes the progress in the luminosity measurement made by DELPHI since the published results of the 1990 data [1]. The major steps of improvement are the following:

- the published 1990 Small Angle Tagger luminosity data were re-analysed, leading to a smaller systematic uncertainty on the overall normalization;
- the absolute luminosity in 1991 was measured with the SAT with still better accuracy than in 1990;
- the 1991 relative point-to-point luminosity was also derived from the Bhabha rate measured with the Very Small Angle Tagger [6], for which the visible cross section is more than 15 times larger than for the SAT. This permits a reduction of about 20% in the statistical uncertainties on the mass and the total width of the  $Z^0$ .

### 4.1 The SAT Measurement

The SAT luminosity measurement is based on the observation of small angle Bhabha scattering in calorimeters consisting of lead sheets and plastic scintillating fibres, covering the polar angle range from 43 to 135 mrad. The fiducial region is accurately defined by a precisely machined lead mask in front of one of the calorimeters. An additional “ $\phi$  mask” covers  $\pm 15^\circ$  around the vertical junction between the two calorimeter half-barrels. Improvements to the detector and the analysis since the published results of the 1990 data [1] are pointed out below.

#### 4.1.1 SAT Triggers

The triggers for luminosity events were based on pulse-height sums of 24 channels in 24 overlapping sectors of  $30^\circ$  per endcap. The primary Bhabha trigger required a coplanar coincidence of energy depositions, each above 12 GeV (10 GeV in 1990). A secondary Bhabha trigger introduced for the 1991 data taking required a coincidence of energy depositions above 30 GeV without the coplanarity requirement. In order to measure the Bhabha trigger efficiency, events with a single energy deposition above 30 GeV were triggered and, to keep the rate to a tolerable level, a fraction was selected for readout. Of the 9867 selected Bhabha events for which the single arm trigger was active, none were missing the coincidence requirement. In addition, the fraction of Bhabha events without the primary Bhabha trigger but with the secondary one was less than  $10^{-4}$ . The primary trigger was thus essentially 100% efficient with a statistical accuracy of about 0.02%.

A “delayed Bhabha” trigger (coincidence in one calorimeter with the other arm from a different beam crossing) with the same 30 GeV thresholds and lack of coplanarity requirement as the secondary Bhabha trigger, was used to monitor the off-momentum electron background during 1991. A similar trigger with 10 GeV thresholds was active in 1990 but the relatively large rate made an extrapolation to the sample of selected Bhabha events very uncertain.

#### 4.1.2 Event Selection

The event selection was based on the reconstructed energies and positions of the showers with the maximum number of readout elements in each calorimeter. A study of radiative Bhabha events with three reconstructed showers showed that the fraction of accepted Bhabha events in which the showers with maximum energy did not also have the maximum number of readout elements was less than  $10^{-4}$ . The acceptance was defined by the following selections on showers:

1. radius in the masked calorimeter inside the outer ring of readout elements;
2. radius in the unmasked calorimeter more than 2.5 cm from the inner edge;
3. less than half of the shower energy in the masked calorimeter in the inner ring of readout elements;
4. energy in each calorimeter greater than  $0.65 \times E_{beam}$ ;
5.  $\phi$  angle in the masked calorimeter more than  $8^\circ$  from the vertical ( $y$ ) axis.

Selections 1 and 2 were performed with the shower centroids but the precision of these selections was improved in the 1991 data by calibrating the calorimeter geometry to that of the silicon tracker (see Section 4.1.3). Selection 3 and, to a lesser extent, selection 4 were based on the effect of the acceptance masks on the energy deposition in the calorimeter. Selection 5 was used to reject the background caused by the tail of the showers penetrating the  $\phi$ -mask and the gap between the calorimeter halves and producing spurious energy depositions in the photodiode readout system. By scanning rejected events the systematic uncertainty was estimated to be about the same as the fraction of the data removed by selection 5, namely 0.15%.

A correction was applied for a non-linear energy response which is not included in the detector simulation. The correction function was fitted to the peak in the Bhabha energy distribution as a function of the LEP centre-of-mass energy. The low energy behaviour of this parameterization is in agreement with test beam data (3 - 9 GeV) taken with one of the calorimeter modules in November 1990, and with the total energy seen in fully reconstructed  $e^+e^-\gamma$  events. The effect of this correction together with the softer energy spectrum predicted by BHLUMI [7] brings the distribution of the minimum of the two primary shower energies of the data into excellent agreement with the simulation. The uncertainty due to selection 4 is reduced to 0.25%, compared to the 0.4% estimated for the original analysis of the 1990 data. This 0.25% error arises from the residual uncertainty in the non-linear behaviour and the difficulty of resolving the separate components of the low energy tail due to radiation, the edges of the masks and the details of the calorimeter response.

During the shutdown of LEP between 1991 and 1992 the geometry of the mask system was measured on a 3-D measurement machine that was precise to  $3 \mu\text{m}$ . The masks were measured before and after dismounting and mounting both the calorimeter halves and the two halves of the masks system several times. As a result of these measurements and cross-checks with the detector geometry in the simulation, the luminosity had to be corrected by +0.84%. A precision similar to the one quoted in ref. [1] (0.15%) is

estimated, but with an additional term of the same size to account for the observed non-reproducibility of the mounting operation.

### 4.1.3 The SAT Silicon Tracker

In 1991 a two-plane silicon tracker with radial pitch 1 mm and azimuthal segmentation of  $5^\circ$  was introduced and operated for one third of the beam crossings during the first 65% of the data taking. Distortions in the calorimeter position reconstruction were measured by the tracker in events in which there were unambiguous 2-hit tracks pointing to the impact point reconstructed by the calorimeter. In this way the two 0.25% uncertainties [1] on the acceptance cuts made by the calorimeter at the minimum scattering angle opposite the mask and the maximum scattering angle in the masked calorimeter are reduced to a single uncertainty of 0.1%. The residual uncertainty is primarily due to the conservatively estimated 400  $\mu\text{m}$  uncertainty in the diameter of the tracker and the limited statistics of the data sample with the tracker active.

### 4.1.4 Backgrounds

The background of Bhabha events producing spurious large energy depositions below the acceptance of the ring mask was reduced by a factor of two in 1991 by inserting 13 mm thick cylindrical lead masks inside the calorimeters. This shielding also served to reduce the single arm trigger rates, leading to an improved measurement of the trigger efficiency.

Backgrounds from two-photon processes and  $e^+e^- \rightarrow \gamma\gamma$  were calculated and found to be negligible. The accidental coincidence of high energy off-momentum electrons was studied with various techniques with the following results:

1. The rates of single off-momentum electrons in each calorimeter were separately measured. The probability of an accidental coincidence was calculated from these rates to be less than 0.01%.
2. Extrapolating the tails of the acoplanarity distribution through the  $\pm 20^\circ$  region of the signal gave an upper limit for the background of 0.01%.
3. The number of delayed Bhabha triggers was less than 0.1% of the number of accepted Bhabha events. In addition, only a small fraction of the single showers (due to the nature of the trigger, it was not possible to read out both of the calorimeters) in the delayed Bhabha events fell within the geometric acceptance of the luminosity measurement.

### 4.1.5 The Theoretical Cross Section

The luminosity is the number of selected Bhabha events, corrected for backgrounds and inefficiencies, divided by the theoretical cross section into the SAT acceptance, that is the visible cross section  $\sigma_{vis}$ . The calculation of  $\sigma_{vis}$  was based on the detailed simulation of Bhabha events produced by the  $\mathcal{O}(\alpha)$  event generator BABAMC [8]. Higher order corrections were calculated with the event generator BHLUMI V2.01 [7]. The uncertainty in the theoretical cross section is estimated to be 0.3%, which includes the 0.25% estimate of Jadach and co-workers [7] plus an additional contribution of 0.1% added because the higher order corrections were made by reweighting the BABAMC events. The reweighting was done according to the unsmearred minimum energy spectrum of the events accepted by the analysis cuts. The electroweak corrections were computed with BABAMC and confirmed by the calculation in ref. [9].



The event generation and detector simulation were carried out at a centre-of-mass energy of 91.1 GeV. The visible cross section was found to be 27.09 nb, including higher order and electroweak corrections. The extrapolation to other energies was performed by correcting for the  $1/s$  dependence of QED and the energy variation of the electroweak effects [7,9]. Ten times more simulated events, concentrated in the critical regions, were used for this analysis than for the published 1990 results [1].

#### 4.1.6 Results

The 1990 data have been re-analysed with the new corrections described above. The net effect is to increase the 1990 luminosities by between 1.4% and 1.8%. A summary of the uncertainties published for the 1990 data and new estimates of the uncertainties for both the 1990 and 1991 data is given in Table 1. The experimental uncertainty for the 1991 data is common to the improved result for 1990.

Contribution	Uncertainty (%)		
	90	90'	91
Mask radius	0.15	0.21	0.21
$\phi$ acceptance	0.10	0.17	0.14
Unmasked acceptance borders	0.35	0.10	0.10
Interaction point position	0.13	0.13	0.13
Energy cut	0.40	0.25	0.25
Fake high energy deposits at small radii	0.16	0.16	0.08
Data behind $\phi$ -mask	0.15	0.15	0.15
Less than half of energy in inner ring	0.10	0.10	0.10
Monte Carlo statistics	0.15	0.03	0.03
Trigger efficiency	0.13	0.13	0.02
Off-momentum background	0.14	0.14	0.05
Dead channel correction	0.16	0.16	0.10
Miscellaneous	0.30	0.20	-
Total experimental	0.8	0.6	0.5
Theory	0.5	0.3	0.3
Total systematic uncertainty	0.9	0.7	0.6

Table 1: Contributions to the systematic uncertainty on the SAT luminosity measurement. The previously published 1990 results and the results of the improved data analysis are shown in columns 90 and 90', respectively.

## 4.2 The VSAT Measurement

The Very Small Angle luminosity monitor of DELPHI (VSAT) was used for the 1991 data taking, but not in 1990. It measures the Bhabha scattering rate between 5 and 7 mrad in polar angle and covers effectively about  $180^\circ$  in azimuth due to the focusing of the low  $\beta$  quadrupoles.

Because of the angular coverage of the VSAT, the replacement of the SAT luminosity by the VSAT luminosity in the computation of the hadronic  $Z^0$  lineshape cross sections allows for a more accurate determination of the mass and the total width of the  $Z^0$ . This improvement has two origins:

- the contribution of the Bhabha statistics to the statistical uncertainty in the cross sections, which is still sizeable for the hadronic lineshape determined with the SAT luminosity, becomes almost negligible;
- the contribution of the electroweak interference to the visible cross section of the VSAT is negligible, contrary to the SAT which measures Bhabha events produced at larger polar angles. Thus the lineshape determined with the VSAT luminosity is free of uncertainties related to the lack of knowledge of the energy dependence of the electroweak interference.

As to the absolute luminosity, the systematic errors, mainly connected to absolute geometrical uncertainties and to theory, are larger for the VSAT than for the SAT. Therefore, for the purpose of the present lineshape determination, the data taken at the  $Z^0$  peak are used to normalize the VSAT data to the SAT absolute luminosity.

A brief description of the detector is given below, followed by the main features of the analysis. More details can be found in ref. [6].

The detector consists of 4 small electromagnetic calorimeter modules located symmetrically in the horizontal plane around an elliptical section of the LEP beam pipe at 7.7 m on each side of the intersection point, immediately behind the low  $\beta$  superconducting quadrupoles.

The detector modules contain 12 tungsten absorbers of 2 radiation lengths, each interspaced with 11 full area silicon planes (FAD) for the energy measurement. The energy resolution for transversely contained showers is  $35\%/\sqrt{E(\text{GeV})}$ . The electromagnetic shower coordinates, in the horizontal ( $x$ ) and vertical ( $y$ ) directions, are given by silicon strip planes with 1 mm pitch placed at 5 ( $x$ -plane), 7 ( $y$ -plane), and 9 ( $x$ -plane) radiation lengths, i.e. close to the shower maximum. The position resolution is about 200  $\mu\text{m}$ .

The Bhabha selection was based on the following requirements:

- trigger coincidence between the modules on opposite sides of DELPHI, requiring an energy deposition of at least 20 GeV in the central nine planes of each module;
- energy of both electrons larger than 70% of the beam energy;
- reconstructed  $x$  and  $y$  positions of both electrons at least 1 mm from the detector edges.

The analysis of events triggered by delayed back-to-back coincidences showed that the background due to accidentals amounted to about 0.3%.

Various simulations based on the BABAMC generator [8] were used as an overall cross-check of the performance of the detector and for producing a matrix which allowed the extraction of beam dependent corrections to the detector acceptance. The parameters which need to be considered are:

- interaction point position ( $x$ ,  $y$  and  $z$ );
- beam tilt ( $x'$ ,  $y'$ );
- beam width ( $\sigma_x$ ,  $\sigma_y$ );
- beam divergence ( $\sigma_{x'}$ ,  $\sigma_{y'}$ );
- quadrupole current (obtained from the low- $\beta$  settings).

To determine the beam position, size, divergence and tilt, the distributions in  $x$  and  $y$  of the centroids of the showers produced by the Bhabha events measured in the strip planes were analysed. Several features of these distributions are strictly correlated to the beam parameters:

- the mean value of the difference in  $x$  between the opposite modules of each diagonal arm,  $\overline{\Delta x}$ , is mainly related to the beam position in  $x$ ;

- the width of the  $\Delta x$ -distribution,  $\sigma_{\Delta x}$ , is mainly related to the beam divergence in  $x$ ;
- the rate asymmetry,  $asy$ , between the two diagonal arms is related to the tilt in  $x$ ;
- similar beam parameters can be extracted in  $y$ , although the values are smaller and the sensitivity much less.

The VSAT position measurements of the Bhabha pair can also be used to measure the location of the interaction point in  $x$ ,  $y$  and  $z$ .

To correct for the variation of the accepted cross section as a function of the beam parameters, the values of the observables ( $\Delta x$ ,  $\sigma_{\Delta x}$ ,  $\Delta y$ ,  $\sigma_{\Delta y}$ ,  $asy$ ) were averaged over approximately 2500 Bhabha events, corresponding to about  $5 \text{ nb}^{-1}$  of integrated luminosity. The correction was expressed as an analytic function of these variables (and of the  $\beta$  setting parameters), with coefficients determined by the simulation program. The major systematic errors are due to the corrections, and include the statistical and systematic error on the observables, the errors on the correction coefficients, the uncertainty from the detector edge cut, the energy cut and the trigger stability. Table 2 summarizes the various contributions to the systematic error.

Errors from the correction factors do not scale with statistics. However, they average out when summing over all the data taken at a given energy point, leaving only a small residual.

The measurement errors which affect the values of the observables used to determine the corrections due to variations in the beam parameters arise from:

- a statistical uncertainty related to the size of the data sample used to determine the values of the observables;
- biases in the position reconstruction, due to fluctuations in the strip calibration constants, position reconstruction inefficiencies, etc.. Such fluctuations have been monitored in each machine fill and found to have a completely negligible effect on the accepted cross section, except for the detector edge cut which is discussed below;
- rapid variations of beam parameters such as the position or divergence, on a time scale of a few seconds or minutes, which cause a broadening of the measured distributions. The effect of this on the acceptance was estimated by comparing the integrated luminosity calculated with acceptance corrections evaluated as above, to the luminosity of the same data sample with the corrections evaluated for a three times larger set of Bhabha events around a given data point. For a typical machine fill, the comparison shows a difference of 0.03% in the calculated acceptance for  $\Delta x$  and of 0.08% for  $\sigma_{\Delta x}$ .

Uncertainties related to the fiducial region cut are dominated by the definition of the inner edge of the detector, where the rate is highest. Since events with maximum signal on the first strip are rejected, any fluctuation in the calibration constants of the first two strips will cause fluctuations in the number of accepted events. An uncertainty in the luminosity of 0.04% at each energy point is attributed to this effect.

The energy calibration constants are rather stable and provide an absolute energy measurement within 0.5%. However, to reduce the fluctuations in the accepted events, the detector was recalibrated for each machine fill to the beam energy. The conservatively estimated 0.5% calibration uncertainty results in a 0.02% uncertainty for each energy point.

The remaining errors due to variations in trigger efficiency and background subtraction are negligible. The trigger efficiency was found to be very stable and larger than 99.9%.

Contribution	Uncertainty (%)
Errors from correction factors	0.07
Uncertainty from errors on measured parameters	0.04
Detector edge cut	0.04
Energy cut	0.02
Trigger efficiency, Bhabha selection	0.01
Total uncorrelated systematic error	0.07
Total correlated systematic error	0.06
Total systematic error	0.09

Table 2: Contributions to the systematic error of the VSAT luminosity.

For each energy different from the peak energy, the quadratic sum of the systematic errors mentioned above amounts to 0.09%, where 0.07% is independent from energy to energy and 0.06% is common to all energy points. For the cross section computations described in Sections 5 and 6, the uncorrelated 0.07% error was convoluted quadratically with the statistical error of the cross section at each energy, whereas the 0.06% correlated error was added quadratically to the SAT normalization uncertainty, which includes the statistical uncertainty on the SAT measurements.

## 5 Hadronic Event Selection and Cross Sections

### 5.1 Selection Criteria

The event selection of the 1991 data was based on charged particles only for which the selection criteria were similar to those used in ref. [1], namely:

- momentum larger than 0.4 GeV;
- relative error on momentum measurement below 100%;
- track length larger than 30 cm;
- projection of impact parameter to the nominal interaction point in the plane transverse to the beam direction ( $r$ ) below 4 cm;
- distance from the nominal interaction point to the vertex of the event along the beam direction ( $z$ ) below 10 cm;
- polar angle  $\theta$  between  $20^\circ$  and  $160^\circ$ .

The cut on the polar angle was introduced because the tracking efficiency was low at small polar angle and is poorly reproduced by the simulation at present. Small, momentum dependent, corrections were applied to the simulated charged particles between  $20^\circ$  and  $30^\circ$ , between  $150^\circ$  and  $160^\circ$  and around  $90^\circ$ . They reflect the observed detection and reconstruction inefficiencies in these angular ranges. However the azimuthal distribution of charged particles is adequately described by the simulation and no correction was needed.

Events were retained as hadronic if the charged multiplicity ( $N_{ch}$ ) was at least 5 and if the total charged energy ( $E_{ch}$ ) was greater than 12% of the centre-of-mass energy. The measured and simulated distributions of charged multiplicity and energy are shown in Figure 1. A satisfactory agreement is obtained once all relevant backgrounds described in Section 5.3 are subtracted. The residual discrepancy observed for medium and large

values of  $E_{ch}$  is mainly attributed to differences in momentum resolution and tracking efficiency between reality and the simulation, with a smaller fraction of the discrepancy coming from the choice of the generators and fragmentation functions used in the Monte Carlo program.

## 5.2 Selection Efficiency

With these criteria the event selection efficiency was estimated to be 94.66% at the peak collision energy, including a decrease of  $(0.21 \pm 0.07)\%$  due to the correction applied to simulated charged particles between  $20^\circ$  and  $30^\circ$  and between  $150^\circ$  and  $160^\circ$  as well as around  $90^\circ$  in polar angle.

Samples of  $10^6$  hadronic events were generated with a fast detector simulation [10] at 7 different centre-of-mass energies, ranging from 88 to 94 GeV. A small variation of the selection efficiency as a function of the collision energy was observed, which is due to the combined effect of the increase of  $N_{ch}$  and of the decrease of  $E_{ch}/\sqrt{s}$  with growing collision energy. The efficiency is highest at the peak collision energy and lowest at the smallest collision energy, where it is about 0.07% smaller than at the peak.

The main components of the uncertainty in the selection efficiency are listed in Table 3. In order to evaluate the uncertainties related to the selection criteria, the cross sections were computed for various values of the cuts on the charged multiplicity and energy ( $N_{ch}$  and  $E_{ch}$ ). By varying the cut on  $N_{ch}$  from 5 to 7 (or 6), the cross sections vary by  $(0.12 \pm 0.01)\%$  (or  $(0.040 \pm 0.007)\%$ ). By varying the cut on  $E_{ch}$  from 12% to 16% (or 14%) of the collision energy, the cross sections vary by  $(0.050 \pm 0.001)\%$  (or  $(0.050 \pm 0.005)\%$ ). From this we conclude that the uncertainties associated with the cuts on  $N_{ch}$  and  $E_{ch}$  amount respectively to 0.12% and 0.05%, common to all collision energies.

In order to study the consequence of the residual discrepancy between data and simulation in the charged energy distribution, the momenta of simulated charged particles were smeared in order to make the discrepancy almost vanish. The observed change in selection efficiency was 0.01%. Another study was performed, where the cross sections were computed at each collision energy from events having a reconstructed thrust axis between  $45^\circ$  and  $135^\circ$  with respect to the beam axis. For these specific events, uncertainties related to reconstruction inefficiencies and reinteractions in the detector material are significantly reduced, as well as the contamination by Bhabha and two-photon collision events. No significant difference with the standard values of the cross section was observed. A 0.1% uncertainty is attributed to the residual discrepancies between the real and simulated distributions of  $N_{ch}$  and  $E_{ch}$ .

Error source	Error (%)
Monte Carlo statistics	0.03
Correction for inefficiencies	0.07
Charged multiplicity	0.12
Charged energy	0.05
Residual data/Monte Carlo discrepancies	0.10
Total	0.18

Table 3: Contributions to the uncertainty on the hadronic event selection efficiency.

The total systematic uncertainty on the selection efficiency was estimated to be 0.18%. This is less than the 0.4% quoted in ref. [1], mainly because of a tuning of the Monte

Carlo generation parameters, of a better simulation of the secondary interactions in the detector material and a better understanding of the momentum resolution. These improvements result in a better agreement between simulated and measured charged energy and multiplicity distributions.

A total of 243,000 events was selected in 1991, corresponding to an integrated luminosity of  $10.7 \text{ pb}^{-1}$ .

### 5.3 Backgrounds

All backgrounds were re-evaluated for this analysis. The contamination from  $\tau^+\tau^-$  pairs was found to be  $(0.40 \pm 0.01)\%$  from a simulated sample of about  $10^5$  pairs based on the KORALZ [11] event generator. This rate was also determined by analysing the events with charged multiplicity 5 or 6. The thrust, the acollinearity and the invariant mass of the group of charged particles (assumed to be pions) found in each hemisphere (defined with respect to the thrust axis) of these events were computed for the real data and for simulated  $q\bar{q}$  and  $\tau^+\tau^-$  samples. The measured distributions could only be reproduced if  $(0.50 \pm 0.01)\%$   $\tau^+\tau^-$  pairs were added to the  $q\bar{q}$  Monte Carlo sample. This can be seen in Figure 2, where the distributions of the thrust, of the acollinearity and of the invariant mass per hemisphere are shown for real and simulated data. Therefore, from the average of the two methods, the residual background due to  $\tau^+\tau^-$  pairs was estimated to be  $(0.45 \pm 0.05)\%$ .

Because of photon radiation and conversion pairs produced in the beam pipe and detector material, a small fraction of  $e^+e^-$  events passed the hadronic selection criteria. The magnitude of this background was evaluated from the simulation of 30,000 events with the BABAMC [8] generator, taking into account the centre-of-mass energy dependence of the cross section. The background was found to be largest at the lowest collision energy, where it amounts to 0.2%, and is smallest at the peak energy, where it amounts to only 0.04%.

The background from  $\mu^+\mu^-$  pairs was also evaluated. From a sample of 41,000 fully simulated  $\mu^+\mu^-$  events generated with the DYMU3 [12] generator, the contamination was found to be less than 0.01% at all collision energies.

The background from two-photon collisions was estimated from a sample of 70,000 fully simulated events, based on a generator including quark-parton, QCD and vector-meson contributions [13]. The contamination was found to be  $10 \pm 5 \text{ pb}$  at each scan point. This is less than the  $20 \pm 10 \text{ pb}$  contamination of the 1990 data mainly because of the cut on the track polar angle applied to the 1991 data.

Finally, the background due to beam-gas and beam-wall interactions was found to be less than an equivalent of 2 pb at each collision energy.

The contaminations from the different sources mentioned above are summarized in Table 4.

### 5.4 Cross Section Computation

The hadronic cross section was computed as previously at each energy from the relation:

$$\sigma_h(s) = \frac{N_h - N_b}{\epsilon \cdot L} \cdot (1 + f_{sm}), \quad (1)$$

where  $N_h$  stands for the number of selected hadronic events,  $N_b$  is the number of background events,  $L$  stands for the time integrated luminosity,  $\epsilon$  is the overall efficiency for

Background source	Contamination	Error
$\tau^+\tau^-$	0.45%	$\pm 0.05\%$
$e^+e^-$	0.04 – 0.2%	negligible
$\mu^+\mu^-$	$< 10^{-4}$	negligible
two-photon collisions	10 pb	$\pm 5$ pb
beam-gas/wall interactions	$< 2$ pb	negligible

Table 4: Magnitude of the different backgrounds with their uncertainty.

hadronic events, and  $f_{sm}$  is an  $s$ -dependent correction factor due to the spread in the collision energy mentioned in Section 2. This factor is calculated using an approximate lineshape and is applied to all cross sections reported in this paper.

The mean collision energy of each of the 16 scan points was taken as the luminosity weighted average of the energies of all the selected accelerator fills around a given scan point. The 1990 values of the centre-of-mass energy [1] were corrected for the new evaluation of the energy mentioned in Section 2.

After subtracting the contamination due to two-photon collisions and  $e^+e^-$  and  $\tau^+\tau^-$  events, the cross sections shown in Table 5 were obtained. The 1990 cross section measurements [1] were corrected for the contamination by  $e^+e^-$  events and for the new determination of the SAT luminosity described in Section 4.1. The absolute luminosity used in the computation of the 1991 cross sections was also provided by the SAT but the relative point-to-point luminosities were obtained from the VSAT measurements. The errors quoted are only statistical except for the 1991 data where they include those VSAT systematic uncertainties (about 0.07%) which are independent from point to point.

The overall 1991 (1990) normalization error is 0.2% (0.4%) from efficiency and backgrounds, in addition to the 0.6% (0.7%) error in the absolute luminosity measurement. The 1991 cross sections were also computed with the SAT luminosity at each energy point and found to be in agreement with the values based on the VSAT luminosities. The reduction of the statistical error on the cross sections when the SAT luminosity determination is supplemented by that of the VSAT ranges from 28% near the resonance peak to 8% at 88.464 GeV.

The integrated luminosities for each scan point are given in Table 5, together with the number of selected hadronic events. The total integrated luminosity for the combined 1990 and 1991 data samples is  $16.1 \text{ pb}^{-1}$  and the total number of selected hadronic events is 356,000. The hadronic cross sections are given in Table 5 and plotted in Figure 3.

## 6 Leptonic Event Selections, Cross Sections and Forward-Backward Charge Asymmetries

The 1990 cross section measurements [1] were corrected for the new determinations of the luminosity described in Section 4.1. The analyses of the 1991 data are similar to those applied to the 1990 data [1], but with the improvements outlined below.

In the following the forward-backward charge asymmetry is defined as :

$$A_{\text{FB}}^f = \frac{\sigma_{\text{F}}^f - \sigma_{\text{B}}^f}{\sigma_{\text{F}}^f + \sigma_{\text{B}}^f},$$

Collision energy (GeV)		Cross sections (nb)	Integ. L. (nb <sup>-1</sup> )	Number of events
1990	1991			
88.223		4.48 ± 0.12	367.5	1602
	88.464	5.15 ± 0.09	711.1	3495
89.222		8.48 ± 0.16	444.1	3655
	89.455	9.99 ± 0.13	632.7	6023
	90.208	17.86 ± 0.18	622.6	10589
90.217		18.00 ± 0.28	389.0	6777
	90.240*	18.83 ± 0.61	56.8	1018
	91.208	30.10 ± 0.12	2482.5	70993
91.217		30.54 ± 0.15	2831.7	83311
	91.239*	29.96 ± 0.09	4221.8	120190
	91.953	24.78 ± 0.21	666.1	15702
92.209		21.57 ± 0.31	423.0	8803
	92.953	14.12 ± 0.16	634.6	8531
93.208		12.58 ± 0.20	467.2	5685
	93.702	10.07 ± 0.13	681.2	6536
94.202		7.82 ± 0.15	470.9	3565

Table 5: DELPHI hadronic cross sections measured in 1990 and in 1991. The two 1991 pre-scan points are marked with a star. The uncertainties quoted are statistical. They do not include overall normalization uncertainties coming from efficiencies and backgrounds (0.2% in 1991, 0.4% in 1990) and from the absolute luminosity (0.6% in 1991, 0.7% in 1990).

where  $\sigma_F^f$  ( $\sigma_B^f$ ) is the cross section for the production of a charged lepton  $f^-$  with  $\cos\theta > 0$  ( $< 0$ ), where  $\theta$  is the polar angle of the  $f^-$  with respect to the incident  $e^-$  direction.

## 6.1 $e^+e^-$ Event Selection

Two independent methods have been developed to analyse the reaction  $e^+e^- \rightarrow e^+e^-$  in order to increase the overall selection efficiency and to obtain a better determination of the efficiency corrections. For both analyses, events were accepted if both final state charged particles had a polar angle between  $44^\circ$  and  $136^\circ$ , and their acollinearity was smaller than  $10^\circ$ .

### 6.1.1 Method 1

This is essentially the method used to analyse the data collected during 1990. Events were accepted if they contained:

- two back-to-back high energy clusters in the barrel electromagnetic calorimeter (HPC), at least one with energy above 30 GeV, the other above 25 GeV;
- no more than 4 charged particles with momentum above 1.5 GeV and with impact parameter to the average interaction point smaller than 5 cm both in the radial and in the beam direction. Events with 1–3, 0–3 or 0–4 topologies were selected only if the total electromagnetic energy was greater than 70 GeV;



- hits in the VD compatible with one charged track per hemisphere in topologies 0–0 and 0–1.

To avoid possible small losses of events due to bad reconstruction of one shower in the HPC, events were also accepted with :

- one very energetic electromagnetic cluster with energy above 40 GeV;
- at least one charged particle in each hemisphere;
- no energy deposited beyond the first 1.5 interaction lengths of the Hadron Calorimeter.

The energy cuts quoted were used at the peak energy; they were scaled according to the event centre-of-mass energy at the other scan points. Since this selection was essentially based on the HPC, the regions in polar and azimuthal angles where this detector has gaps between modules were excluded from the analysis.

Two improvements were introduced with respect to the analysis of reference [1]. First, the three layers of the microvertex detector were used to count, with full azimuthal coverage, the particles originating from the vertex. In this way, annihilation events into two photons were rejected with almost 100% efficiency, and negligible loss of efficiency in the  $e^+e^-$  selection. Second, the improvement in the detector simulation allowed the fiducial region to be extended down to  $\pm 0.7^\circ$  in  $\phi$  from the HPC gaps (compared to  $\pm 1.0^\circ$  used in the past). The cut in polar angle at  $(90 \pm 2)^\circ$  was maintained.

A total of 6670 events was selected with this analysis. The selection efficiency was estimated to be  $(89.71 \pm 0.23)\%$  using a sample of 21642 simulated  $e^+e^-$  events in the  $\theta$  acceptance region. This value does not include the loss due to the exclusion of the  $4^\circ$  polar angle region around  $90^\circ$  which amounted to about 4% (depending on energy), because this was computed using two independent programs ALIBABA [14] and TOPAZ0 [15].

With a sample of 38131 simulated  $\tau^+\tau^-$  events, the percentage of  $\tau^+\tau^-$  events passing the selection cuts was estimated to be  $(1.46 \pm 0.07)\%$ . Backgrounds from other sources were estimated to be negligible.

The final result is not completely stable against variations of the cuts used to select the events. These instabilities are attributed to the non-perfect modelling of the simulated events, with effects both on the selection efficiency and on the background estimations. By varying the energy cut values by  $\pm 20\%$ , the systematic error from this effect is evaluated to be 0.25%. Small additional contributions to the systematic error come from the trigger efficiency and from the acceptance region definition ( $\pm 0.20\%$ ). The overall systematic error of the cross sections obtained with this method is found to be  $\pm 0.40\%$ , to be added to the uncertainty in the luminosity.

### 6.1.2 Method 2

In this method,  $e^+e^-$  events were selected with two independent sets of experimental cuts, chosen in such a way as to minimize the correlations between the two sets. As in method 1, a cut in polar angle at  $90 \pm 2^\circ$  was applied. In one set (selection A), events were accepted if they had :

- at least two opposite track segments seen by the microvertex detector (VD) and no more than four in total;
- two high energy electromagnetic clusters observed in the HPC, at least one with energy above 35 GeV and another above 25 GeV. If the most energetic cluster pointed to within  $2^\circ$  of a gap in the HPC, then the energy of the second cluster was

defined as the HPC energy plus the energy measured in the first layer of the barrel HCAL. In this case there should be no energy in layers 3 and 4 of the barrel HCAL.

In the second set (selection B), events were accepted if they had:

- at least 2 charged particle tracks, of momentum greater than 1.5 GeV and distance of closest approach to the nominal vertex position less than 5 cm, seen by the DELPHI tracking system (except VD) with acollinearity less than  $10^\circ$ , and no more than four tracks in total;
- the sum in quadrature of the momenta of the highest momentum charged particles in each hemisphere greater than 45 GeV;
- the ionization, as measured by the TPC, of all tracks in the event compatible with the electron hypothesis;
- no energy observed in the last three layers of HCAL associated to the impact points of the two highest momentum charged particles;
- the Outer Detector hit pattern associated to the impact points of the tracks incompatible with the pattern of a non-showering particle;
- no hit in the muon chambers associated to the tracks.

As in the previous analysis, the energy cut values were scaled with the centre-of-mass energy of the events.

In total, 7203 events were selected with this method. Considering the selections A and B as independent, the efficiency of each of them and their overall efficiency can be easily computed by a comparison of the number of events selected by each one separately or by both simultaneously. To get a correct result, the contribution of background events passing the cuts had first to be subtracted. The presence of background in the sample of selected events has two consequences. First, it increases the number of selected events, second it biases the estimate of the selection efficiency towards smaller values. Using the  $\tau^+\tau^-$  simulated events quoted in the discussion of method 1, the percentage of tau events passing the cuts was found to be 0.55% for selection A and 0.73% for selection B, with only 0.04% of events passing both selections. Backgrounds from other sources were estimated to be negligible. After the background correction, the overall efficiency of the two selections was measured to be  $(97.10 \pm 0.14)\%$ . No evidence of variation of this number with centre-of-mass energy was observed, the measurements being completely consistent with statistical fluctuations about a constant value. This measured efficiency does not include the loss due to the exclusion of the polar angle region around  $90^\circ$ . The simulated  $e^+e^-$  events were used to estimate and remove the bias caused by the correlation between the two selections due to the detector structure or to the kinematics of the events. The bias on the combined efficiency was found to be less than 0.1%. The final cross section results have a slight dependence on the value of the cuts used in the event selection, mainly on the track momentum cut. By varying the cut values by  $\pm 20\%$ , the systematic error from this effect was estimated to be 0.34%. Adding other small contributions from trigger efficiency and acceptance definition, the overall systematic error with method 2 is 0.42%.

### 6.1.3 Cross Sections and Asymmetries

The cross sections obtained with the two methods are quite compatible. In the following analysis the average of the two results will be used. Taking into account the correlation between the errors of the two measurements, the systematic error on the average was estimated to be 0.37%. To allow a fit of the results with the ZFITTER package [16], the

contribution of the t-channel exchange plus its interference with the s-channel must be removed from the measured cross sections and asymmetries. In addition, ZFITTER only allows a limit on the polar angle of one of the two final state fermions, the other being constrained by the collinearity requirement. These two corrections were computed using the programs, ALIBABA [14] and TOPAZ0 [15]. The two estimates of the t-channel part to subtract from the measured cross sections differed by less than 2 pb at the peak and above, and by less than 1 pb below. The correction for the change of definition of acceptance was small, about 0.5%, but the difference between the estimates of the two programs was about 0.15%. The uncertainties on the t-channel subtraction and acceptance corrections increased the systematic error of the s-channel cross section to 0.5% at the peak. The cross section values before and after the above mentioned corrections are shown in Table 6. The cross sections from the 1990 runs are also included, computed using the new luminosity measurements described in Section 4. Figure 4(a) shows the average cross sections at each centre-of-mass energy, after subtraction of the t-channel contributions. The cross sections in the Figure have been extrapolated to the full solid angle acceptance.

Collision energy (GeV)		Cross sections (s+t) (nb)	Cross sections (s only) (nb)	Integ. L. (nb <sup>-1</sup> )	Number of events
1990	1991				
88.222		0.369 ± 0.039	0.153 ± 0.040	295	95
	88.465	0.331 ± 0.023	0.110 ± 0.023	709	223
89.217		0.487 ± 0.041	0.248 ± 0.041	339	142
	89.460	0.571 ± 0.036	0.326 ± 0.036	488	264
	90.208	0.775 ± 0.039	0.523 ± 0.039	532	387
90.217		0.785 ± 0.053	0.534 ± 0.053	343	229
	91.207	1.033 ± 0.023	0.894 ± 0.023	2314	2253
91.212		1.040 ± 0.023	0.904 ± 0.023	2342	2056
	91.238*	1.064 ± 0.020	0.930 ± 0.020	3178	3185
	91.954	0.784 ± 0.036	0.759 ± 0.036	667	492
92.207		0.612 ± 0.046	0.605 ± 0.046	364	190
	92.953	0.407 ± 0.027	0.412 ± 0.027	604	231
93.206		0.408 ± 0.042	0.413 ± 0.043	286	101
	93.703	0.287 ± 0.023	0.287 ± 0.023	632	168
94.201		0.197 ± 0.024	0.190 ± 0.025	441	78

Table 6: The cross sections, integrated luminosities and number of events for the reaction  $e^+e^- \rightarrow e^+e^-$ , at different centre-of-mass energies. The 1991 pre-scan point is marked with a star. The third column (s+t) gives the measured cross section with both final state fermions in the polar angle range  $44^\circ - 136^\circ$  and acollinearity less than  $10^\circ$ . The fourth column (s only) gives the cross section after t-channel subtraction with only the  $e^-$  constrained by  $44^\circ < \theta(e^-) < 136^\circ$ , and acollinearity less than  $10^\circ$ . The errors are statistical only. The systematic error, excluding luminosity, is, on 1991 data, 0.37% for the s+t cross section, and 0.5% for the s only cross section at the peak. After the re-analysis, the systematic error, excluding luminosity, on the s cross section for the 1990 data is 1.0% at the peak.

The samples of events used in the two methods for the cross section measurement were also used to measure the forward-backward asymmetry  $A_{FB}^e$ . The method used

to determine the charge of the events was similar to the one used for the analysis of the 1990 data [1]. In particular the charge was assigned using the tracking information for events in which the two most energetic particles had opposite charge and using the aplanarity angle between the showers measured in the electromagnetic calorimeter for the other events. Due to the improved track measurement, the percentage of events with two charged particles of the same sign was reduced with respect to the 1990 sample, and was 2.5% of the two-track events. In addition, for almost half of those events, it was possible to determine which particle was assigned the wrong charge using the vertex detector association, the  $\chi^2$  probability of the fit and the value of the measured momentum. Adding also the contribution due to the acceptance definition, the resulting systematic error on the asymmetry measurement was reduced with respect to that of 1990 and was evaluated to be 0.002. The total error induced by the t-channel subtraction, by the precision on the luminosity measurement, by the event selection systematics and by the accuracy of the theoretical computation, is 0.001 at the peak for the runs taken after August 1991, when the scale of the LEP energy is known with the best precision. For the 1991 data taken before August the energy scale error is  $\pm 18$  MeV, and the systematic error on the asymmetry is  $\pm 0.002$  at the peak. The asymmetries at each centre-of-mass energy are shown in Figure 4(b) and Table 7.

Collision energy (GeV)		$A_{\text{FB}}^e$ (s+t)	$A_{\text{FB}}^e$ (s only)
1990	1991		
88.222		$0.460 \pm 0.096$	$-0.04 \pm 0.26$
	88.465	$0.317 \pm 0.067$	$-0.69 \pm 0.28$
89.217		$0.223 \pm 0.084$	$-0.35 \pm 0.19$
	89.460	$0.305 \pm 0.060$	$-0.08 \pm 0.11$
	90.208	$0.165 \pm 0.050$	$-0.148 \pm 0.078$
90.217		$0.177 \pm 0.067$	$-0.12 \pm 0.10$
	91.207	$0.093 \pm 0.022$	$-0.021 \pm 0.026$
91.212		$0.067 \pm 0.022$	$-0.048 \pm 0.026$
	91.238*	$0.122 \pm 0.019$	$0.020 \pm 0.021$
	91.954	$0.125 \pm 0.046$	$0.098 \pm 0.048$
92.207		$0.063 \pm 0.075$	$0.048 \pm 0.076$
	92.953	$0.170 \pm 0.065$	$0.170 \pm 0.065$
93.206		$0.27 \pm 0.10$	$0.263 \pm 0.099$
	93.703	$0.087 \pm 0.078$	$0.071 \pm 0.079$
94.201		$0.20 \pm 0.12$	$0.16 \pm 0.13$

Table 7: The forward-backward asymmetries for the reaction  $e^+e^- \rightarrow e^+e^-$ , at different centre-of-mass energies. The 1991 pre-scan point is marked with a star. The third column (s+t) gives the measured asymmetry with both final state fermions in the polar angle range  $44^\circ - 136^\circ$  and acollinearity less than  $10^\circ$ . The fourth column (s only) gives the asymmetry after t-channel subtraction with only the  $e^-$  constrained by  $44^\circ < \theta(e^-) < 136^\circ$ . The errors are statistical only. The overall systematic error is 0.002 for the s+t asymmetries and 0.003 for the s only asymmetry at the peak for the 1991 data. After the re-analysis of the 1990 data the overall systematic error is 0.003 at the peak.

## 6.2 $\mu^+\mu^-$ Event Selection

The analysis procedure for the selection of candidate  $e^+e^- \rightarrow \mu^+\mu^-$  events in the barrel region was similar to that presented in ref. [1], however improvements in the track efficiency in the forward regions allowed the angular acceptance to be extended. In the present analysis the polar angle range for the determination of cross sections was increased to  $20^\circ < \theta < 160^\circ$  (from  $32.9^\circ < \theta < 147.1^\circ$  in 1990). For the determination of the forward-backward asymmetry the polar angle range was further extended to  $11^\circ < \theta < 169^\circ$  (from  $15^\circ < \theta < 165^\circ$  in 1990). This larger angular acceptance for the asymmetry measurements is important as the size of the error is related to the maximum absolute value of  $\cos\theta$  in the data sample.

Events were retained if they satisfied the following selection criteria:

- there were two charged particles, both having momenta greater than 15 GeV, and coming from the interaction region. The size of this region was dependent on which detectors participated in the track fit. For tracks in which the microvertex detector participated, this region was defined by  $|z|$  less than 4.5 cm and  $r$  less than 0.2 cm. If microvertex measurements were not used, but the TPC or ID participated in the track fit, the accepted region was extended to  $r$  less than 1.5 cm. For other tracks (mainly in the forward region) the requirement was  $r$  less than 5 cm;
- the acollinearity angle between the two charged particle tracks was less than  $10^\circ$ ;
- there were no additional charged particles with momenta greater than 5 GeV, except if the fastest particle had a momentum greater than 40 GeV. The latter requirement reduced the rejection of muon pair events in which the third particle had arisen from radiative effects.

The momentum resolution was considerably improved compared to that of the previous analysis by the inclusion of the 3 layer microvertex detector in the track fit. The momentum resolution was about 4% in the barrel region, where there is microvertex coverage, and rose to about 20% at the extreme values of  $\theta$ . Figure 5 shows the distribution of the electric charge multiplied by the inverse of the momentum. A clear separation of the charges, which is important in the measurement of the forward-backward asymmetry, can be seen. The small tails of the momentum distribution at low values of the inverse momentum are mainly due to reconstructed tracks in which information from one or more of the tracking detectors was not available in the track fit.

Five sub-detectors were used in the muon identification:

- for the MUB and MUF, identification was based on the association of the positions of the muon chamber hits with those expected from the extrapolation of the tracks [17];
- for the HCAL, it was required that the energy deposited was consistent with that expected for a minimum ionizing particle, possibly accompanied by a  $\delta$ -ray or Bremsstrahlung photon; namely that the total energy deposited was less than a cut-off value (which was 10 GeV at  $\theta = 90^\circ$ , increasing to about 15 GeV at  $\theta = 55^\circ$ , and thereafter independent of  $\theta$ ) and that there were energy deposits in at least two of the four layers;
- for the HPC and FEMC it was required that there were energy depositions and that these were consistent with those expected from a minimum ionizing particle (i.e. less than 1 GeV within  $\pm 5^\circ$  in  $\theta$  and  $\pm 10^\circ$  in  $\phi$  around the track extrapolated to the entry point of the calorimeter).

It was required that each particle was identified as a muon by at least one of the sub-detectors mentioned above in either the barrel or forward regions. Events in which one or

both particles were identified as a hadron by the HCAL (deposited energy greater than the above cut-off value) or in which both particles were associated with energy deposits greater than 10 GeV in the HPC or FEMC, and which had an acollinearity angle greater than  $1^\circ$ , were removed. The cosmic ray background was substantially reduced by timing measurements using both the TPC and the OD, by requiring that the tracks observed were consistent with being produced at the beam cross-over time. The cosmic ray background was further reduced with respect to the previous analysis [1] by use of the microvertex detector, which enabled tighter cuts to be made on the distance of closest approach in the transverse plane. This is illustrated in Figure 6 which shows the effect of the inclusion of the microvertex detector. The microvertex detector is included in 98.3 % of the tracks within the geometric acceptance of the detector ( $35^\circ < \theta < 145^\circ$ ).

The identification efficiency of each of the sub-detectors was measured using the data, by counting the number of muon-pairs found by a given sub-detector in a sample defined by the other two sets of sub-detectors. The identification efficiencies were estimated as a function of  $\theta$ . From these studies it was found that the overall muon identification efficiency was  $0.972 \pm 0.002$  over the polar angle range between  $20^\circ$  and  $160^\circ$ . A more restrictive cut on the acollinearity angle was made for the determination of the muon identification efficiency, in order to minimize the effect of the  $\tau$ -background.

The detection efficiencies and the validity of the method of the efficiency determination were cross-checked by generating a sample of  $\mu^+\mu^-$  events using the DYMU3 generator [12] and passing the simulated raw data from the DELPHI detector simulation program [18] through the same analysis chain as for the real data. Simulated events for the  $\tau^+\tau^-$  final state, produced using the KORALZ generator [11], were also analysed for background studies.

### 6.2.1 Cross Section

The cross section for  $e^+e^- \rightarrow \mu^+\mu^-$  was determined for the sample of events in which the negative muon was in the polar angle region between  $20^\circ$  and  $160^\circ$ . It was required that the sub-detector components used in the analysis were fully operational. The number of muon-pair events in this sample was 9786. The total integrated luminosity used for the determination of the cross section was  $10 \text{ pb}^{-1}$ .

In order to determine the cross section the number of events at each energy was corrected for the efficiency of muon identification and by the following factors:

- $1.037 \pm 0.003$ , for loss of muons, either from the dead space of the TPC or in the forward region. The efficiencies were determined using both the data and Monte Carlo simulated events. The error on this correction includes that arising from imprecision on the cuts on the vertex, on momenta and on the polar angle.
- $1.001 \pm 0.001$  for trigger efficiency; this was determined by comparing which triggers fired, on an event by event basis, using triggers derived from independent sets of sub-detectors.
- $0.976 \pm 0.003$ , for the  $\tau^+\tau^-$  background; this was estimated from Monte Carlo simulations as described above.
- $0.998 \pm 0.001$ , at the peak, for the residual cosmic ray background.

The background from the process  $e^+e^- \rightarrow e^+e^-\mu^+\mu^-$ , where the final state  $e^+$  and  $e^-$  remain undetected, was estimated using the event generator described in reference [13]. This background, together with that from  $e^+e^- \rightarrow e^+e^-$ , was found to be negligible.

The cross sections for  $e^+e^- \rightarrow \mu^+\mu^-$ , as a function of the centre-of-mass energy are given in Table 8, and plotted in Figure 7 (a). The total systematic error on the cross

section is 0.5%, in addition to the error on the luminosity. The results for the 1990 data, with luminosity modified as described in Section 4, are also given in Table 8.

Collision energy (GeV)		Cross sections (nb)	Cross sections ( $4\pi$ ) (nb)	Integ. L. (nb <sup>-1</sup> )	Number of events
1990	1991				
88.221			$0.216 \pm 0.032$	316	49
	88.468	$0.227 \pm 0.020$	$0.267 \pm 0.023$	629	137
89.216			$0.416 \pm 0.040$	401	119
	89.461	$0.436 \pm 0.027$	$0.502 \pm 0.030$	647	269
	90.212	$0.750 \pm 0.034$	$0.853 \pm 0.039$	633	448
90.217			$1.073 \pm 0.065$	374	276
	91.210	$1.275 \pm 0.024$	$1.443 \pm 0.028$	2274	2757
91.212			$1.513 \pm 0.031$	2330	2457
	91.243*	$1.293 \pm 0.019$	$1.463 \pm 0.021$	3993	4911
	91.956	$1.120 \pm 0.042$	$1.268 \pm 0.046$	680	725
92.207			$1.159 \pm 0.074$	307	252
	92.956	$0.568 \pm 0.031$	$0.647 \pm 0.036$	634	344
93.209			$0.590 \pm 0.048$	372	155
	93.704	$0.415 \pm 0.030$	$0.477 \pm 0.035$	492	195
94.200			$0.406 \pm 0.038$	413	120

Table 8: The number of selected events, integrated luminosities and cross sections for  $e^+e^- \rightarrow \mu^+\mu^-$  for different centre-of-mass energies measured in 1990 and 1991. The 1991 pre-scan point is marked with a star. For 1991, the results are given in column 3 for the events satisfying the selection criteria that both muon momenta are above 15 GeV, the polar angle of the negative muon satisfies  $20^\circ < \theta < 160^\circ$  and that the acollinearity angle is lower than  $10^\circ$ . The uncertainties quoted are statistical. The total systematic error on the cross section data for 1991 is 0.5%, in addition to the error on the luminosity. The results for 1990 correspond to  $4\pi$  detection and are corrected for the cuts on momenta and acollinearity. The uncertainties quoted are again statistical only. The total systematic error on the cross section is 0.8%, in addition to the uncertainty in the luminosity. Also given in column 4, for convenience, are the 1991 results corrected to  $4\pi$  detection. The 1991 results used in the fits are those from column 3, as the extrapolation to  $4\pi$  introduces an additional theoretical uncertainty.

### 6.2.2 Forward - Backward Asymmetry

For this analysis, events with a detected muon within the polar angle region between  $11^\circ$  and  $169^\circ$ , and which passed the muon pair selection as described above, were used. Since an absolute normalization is not required, less restrictive criteria on the run conditions were applied. Further, the polar angle range was extended to increase the sensitivity of the measured asymmetries. A total of 11465 events was retained from which  $A_{\text{FB}}^\mu$  was extracted at each energy point using a maximum likelihood fit to the angular distribution of the scattered  $\mu^-$ . In the absence of charge-asymmetric and forward-backward asymmetric inefficiencies, this method does not require efficiency corrections. Since the likelihood fit uses the lowest order form for the angular distribution, higher order photonic corrections are not taken into account. Therefore a comparison was made between

the first order form and the differential cross section computed using ZFITTER [16] and applying the experimental cuts described above. The maximal difference observed leads to a common systematic error of 0.001 for all energies. The value of  $A_{\text{FB}}^\mu$  differs by 0.002 using the angle of the scattered  $\mu^+$  for the fit. This effect does not depend on statistical fluctuations of events with hard radiative photons but can be traced back to a different measurement of the angles in both hemispheres. As this systematic difference is not fully understood, the averaged value  $\cos \theta^* = \cos \frac{1}{2}(\theta^- + \pi - \theta^+) / \cos \frac{1}{2}(\theta^- - \pi + \theta^+)$ , where  $\theta^-, \theta^+$  are the polar angles of the negative and positive muons respectively, was used in the computation of the asymmetry. There is a contribution of 0.001 to the systematic error arising from these effects.

The  $A_{\text{FB}}^\mu$  values were also computed by counting the forward and backward scattered  $\mu^-$ , correcting for the  $\cos \theta$  dependent efficiency and extrapolating to the full solid angle, as described in ref. [1]. The values obtained for both methods are listed in Table 9 and show good agreement within the expected statistical difference.

Collision energy (GeV)		Number of events	$A_{\text{FB}}^\mu$ (counting)	$A_{\text{FB}}^\mu$ (likelihood)
1990	1991			
88.221		72	$-0.23 \pm 0.11$	$-0.14 \pm 0.11$
	88.464	152	$-0.269 \pm 0.080$	$-0.267 \pm 0.073$
89.216		162	$-0.17 \pm 0.08$	$-0.21 \pm 0.08$
	89.456	282	$-0.269 \pm 0.059$	$-0.248 \pm 0.054$
	90.211	518	$-0.138 \pm 0.045$	$-0.155 \pm 0.042$
90.217		325	$-0.11 \pm 0.06$	$-0.08 \pm 0.05$
	91.210	3364	$-0.004 \pm 0.018$	$-0.012 \pm 0.017$
91.212		3437	$0.024 \pm 0.017$	$0.007 \pm 0.017$
	91.239*	5674	$0.022 \pm 0.014$	$0.019 \pm 0.013$
	91.954	774	$0.061 \pm 0.037$	$0.065 \pm 0.034$
92.207		387	$0.04 \pm 0.05$	$0.01 \pm 0.05$
	92.952	370	$0.100 \pm 0.053$	$0.105 \pm 0.050$
93.209		217	$0.15 \pm 0.07$	$0.12 \pm 0.07$
	93.701	331	$0.145 \pm 0.056$	$0.156 \pm 0.051$
94.200		163	$0.25 \pm 0.08$	$0.21 \pm 0.08$

Table 9: Measurement of the  $\mu^+\mu^-$  forward-backward asymmetry for different centre-of-mass energies for 1990 and 1991 data. The results are corrected to the full solid angle, but not for the cuts on momenta and acollinearity. The errors are statistical only, the systematic error on these points is 0.005 for the 1990 data and 0.003 for the 1991 data. The 1991 pre-scan point is marked with a star.

The wrong determination of charges was indicated by events with a charge confusion; that is, two muons of apparently the same charge. The data sample contained 24/21 events with negative/positive charges measured in both hemispheres. These events provided a  $|\cos \theta|$  dependent probability that a track was measured with the wrong charge. This led to an estimated relative systematic error of  $\frac{\Delta A_{\text{FB}}^\mu}{A_{\text{FB}}^\mu} = 0.001$  and a maximal error of 0.002, if the maximum possible correlation was considered. The charge acceptance was extracted from the mean values of the momentum distributions for both charges in each hemisphere. Differences may lead to events in the low momentum region being



excluded from the event sample in a way which depends on the charge of the muon. The corresponding systematic error was estimated to be 0.001. A background of 2% of  $\tau^+\tau^-$  events was estimated with a Monte Carlo study of 100,000  $\tau^+\tau^-(\gamma)$  events generated with KORALZ [11] and passing the full detector simulation and analysis chain. The remaining events have a similar asymmetry to the muon data and thus do not cause any significant systematic error. The cosmic ray background contributes mainly to the off peak measurements. The rate and angular distribution of cosmic ray events were estimated by utilizing the region outside the interaction point and extrapolating the results into the interaction region. The values of  $A_{\text{FB}}^\mu$  were corrected for this background and the systematic error from this source was below 0.001. Adding all of these effects in quadrature gave a total estimated systematic error on the asymmetry of 0.003. The results of the asymmetry measurements are given in Table 9 and plotted in Figure 7 (b).

The results of the measurements of  $A_{\text{FB}}^\mu$  for the 1990 data are also given in Table 9; the estimated systematic error on these data is 0.005.

### 6.3 $\tau^+\tau^-$ Event Selection

The analysis for selection of  $Z^0 \rightarrow \tau^+\tau^-$  events differed in a number of respects from that previously presented [1]. The cross sections were estimated with events selected in the polar angle region between  $43^\circ$  and  $137^\circ$  as before but with an improved efficiency and reduced systematic errors. The asymmetry measurements were made with events selected in the extended polar angle region from  $25^\circ$  to  $155^\circ$ . The selection took advantage of the missing energy and momentum carried by the 2 or more neutrinos produced to reject other leptonic decays of the  $Z^0$ , and used the low multiplicity and presence of isolated particles or very collimated jets to reject hadronic events.

The event axis was taken as the thrust axis and the event divided into two hemispheres corresponding to each  $\tau$ . In order that the treatment should be the same independently of the number of charged particle tracks, the most energetic charged particle (leading track) of each side was chosen to define the corresponding  $\tau$  quantities. The leading track in at least one of the hemispheres was required to be in the accepted polar angle range. To define calorimetric energies, a cone of  $30^\circ$  (half opening angle) around the leading track was defined and all energy inside it was added as the  $\tau$  energy.

A first set of cuts was applied to remove  $Z^0 \rightarrow$  hadrons and two-photon events:

$$2 \leq N_{ch} \leq 6, \theta_{iso} \geq 160^\circ, E_{vis} > 8 \text{ GeV},$$

where  $N_{ch}$  is the number of charged particles, as reconstructed in the TPC, coming from a fiducial region around the average interaction point ( $r < 5$  cm and  $|z| < 10$  cm);  $\theta_{iso}$  is the minimum angle between a pair of charged particles in opposite hemispheres and  $E_{vis}$  is the total energy, defined as the sum of the charged particle momenta and neutral electromagnetic energy. The cut in  $\theta_{iso}$  limited the maximum acollinearity in two charged particle events and the opening angle of the jet for higher multiplicity events.

Two further cuts were used to reject leptonic  $Z^0$  decays,  $e^+e^-(\gamma)$  and  $\mu^+\mu^-(\gamma)$ :

$$P_{rad} < 1.0, E_{rad} < 1.0.$$

These two variables are defined as  $P_{rad} = \frac{\sqrt{p_1^2 + p_2^2}}{P_{beam}}$  and  $E_{rad} = \frac{\sqrt{e_1^2 + e_2^2}}{E_{beam}}$ , where  $p_1(p_2)$  and  $e_1(e_2)$  are the momentum and electromagnetic energy assigned to each  $\tau$  as explained above.

Cosmic, beam-gas and beam-wall events were rejected with impact parameter cuts:

$$|z_1| < 4.5 \text{ cm}, |z_2| < 4.5 \text{ cm}, r_1 < 1.5 \text{ cm}, r_2 < 1.5 \text{ cm},$$

where  $r_1$  and  $r_2$  are the impact parameters in the transverse plane of the two leading tracks with respect to the average interaction point and  $z_1$  and  $z_2$  are the distances along the beam between the point of closest approach and the interaction point.

Finally, extra cuts were applied only for 1–1 topology events, to remove remaining background affecting this topology :

$$\theta_{acol} > 0.5^\circ, |\vec{P}_T| > 0.4 \text{ GeV}, |z_1 - z_2| < 3 \text{ cm},$$

where  $|\vec{P}_T|$  is the event transverse momentum relative to the beam axis, and  $\theta_{acol}$  is the acollinearity angle of the two charged particles. The cut on acollinearity reduces the dilepton and cosmic ray backgrounds. The cut on  $|\vec{P}_T|$  reduces the background due to two-photon events. The final cut further reduces the cosmic ray background.

The selection efficiency was determined from Monte Carlo data, produced using KORALZ [11] with detailed detector response simulated, and processed with the standard DELPHI analysis programs, with small corrections for differences found between data and simulation.

The efficiency dependence on centre-of-mass energy was checked by simulating, with a simplified detector response[10], 100,000  $\tau^+\tau^-$  at each of the 7 beam energy points. No deviation greater than expected statistical fluctuations was observed, indicating that the variation in efficiency was less than 0.1%.

By simulation a selection efficiency of  $(52.82 \pm 0.34)\%$  was obtained, equivalent to  $(81.76 \pm 0.53)\%$  within the polar angle region between  $43^\circ$  and  $137^\circ$ . The systematic error on the efficiency arose from the sensitivity to the selections, principally for  $E_{rad}$ ,  $\theta_{acol}$  and  $\theta_{iso}$ . A total of 6528 events was selected.

Backgrounds were estimated from data, and cross-checked with simulated events. The cosmic ray background was estimated to be less than 0.05% using the timing information from the Outer Detector. The overall background was estimated to be  $(1.9 \pm 0.4)\%$  from other  $Z^0$  decays and  $2.0 \pm 0.6$  pb from two-photon and up to 2.1 pb, depending on centre-of-mass energy, from Bhabha processes.

The cross sections are given in Table 10 and shown in Figure 8 (a).

The measurement of  $A_{FB}^\tau$  was made using the maximum likelihood method. The selections used for the cross section measurement were used for the barrel region and a further set of selections introduced for the regions  $25^\circ < \theta < 43^\circ$  and  $137^\circ < \theta < 155^\circ$ . These were:

$$E_{rad} < 0.9$$

and, if both leading tracks lay between the Forward Electromagnetic Calorimeter and the HPC ( $35^\circ < \theta < 43^\circ$  and  $137^\circ < \theta < 145^\circ$ ):

$$P_{rad} < 0.9, \theta_{acol} > 2^\circ,$$

where  $\theta_{acol}$  was defined for all events using the resultant momentum of all particles in each hemisphere. These tight cuts were required to remove  $e^+e^-$  events with a high efficiency in a region with no electromagnetic calorimetry. The average efficiency for the extra events selected outside the barrel was estimated from Monte Carlo simulation to be  $(59.2 \pm 1.0)\%$ . Backgrounds were estimated from Monte Carlo simulation to be  $(6.0 \pm 1.4)\%$ , dominated by the  $e^+e^-$  channel which contributed  $(3.6 \pm 1.0)\%$ . A total of 7916 candidate events was selected.

To calculate  $A_{FB}^\tau$ , it was necessary to reconstruct the  $\tau\tau$  pair production direction and to identify the charges. The thrust axis was used for the direction. Monte Carlo simulations showed that the r.m.s. of the difference between the  $\cos \theta$  of the generated pair

Collision energy (GeV)		Cross sections (nb)	Integ. L (nb <sup>-1</sup> )	Number of events
1990	1991			
88.221		0.218 ± 0.039	327	33
	88.464	0.223 ± 0.025	707	90
89.216		0.455 ± 0.053	363	76
	89.455	0.464 ± 0.038	621	156
	90.209	0.794 ± 0.050	600	267
90.221		0.966 ± 0.076	375	164
	91.208	1.469 ± 0.033	2554	2024
91.213		1.459 ± 0.036	2594	1738
	91.238*	1.470 ± 0.026	3963	3148
	91.952	1.182 ± 0.058	680	430
92.207		0.935 ± 0.074	391	170
	92.952	0.702 ± 0.046	624	236
93.207		0.592 ± 0.065	320	88
	93.702	0.542 ± 0.039	672	195
94.201		0.358 ± 0.042	459	76

Table 10: The number of selected events, integrated luminosities and cross sections for  $e^+e^- \rightarrow \tau^+\tau^-$  for different centre-of-mass energies measured in 1990 and 1991. The results are corrected to the full solid angle. The 1991 pre-scan point is marked with a star. Only statistical errors are shown. The systematic error, excluding luminosity error, is 0.75% for the 1991 data and 1.2% for the 1990 data.

and the measured  $\cos \theta_{thrust}$  was  $\Delta(\cos \theta) = 0.018 \pm 0.004$  ( $\Delta\theta \approx 1^\circ$ ). The uncertainty from the use of the thrust axis to define the event axis was  $\frac{\Delta A_{FB}^\tau}{A_{FB}^\tau} = 0.001$ . A study of the charge identification efficiency in each topology was made using the data and systematic uncertainties due to charge misidentification of  $\frac{\Delta A_{FB}^\tau}{A_{FB}^\tau} = 0.014$  in the barrel and 0.035 in the forward regions were estimated.

Most of the backgrounds did not significantly affect the asymmetry, either because they had a similar behaviour, or because the fraction of these events was too small. However,  $e^+e^-$  t-channel production has a high asymmetry. Its contribution was computed using ZFITTER [16], assuming an uncertainty of 30% of the correction ( $\delta$ ), due to the uncertainty on the total number of events of this type in the selected sample. Systematic effects due to the selection cuts were estimated with 700,000  $\tau^+\tau^-$  events generated at different energies, with the conclusion that such effects give an uncertainty on  $A_{FB}^\tau$  of less than 0.001. Therefore the uncertainty on  $A_{FB}^\tau$  is obtained by a quadratic combination of  $0.014A_{FB}^\tau$  and  $0.3\delta$  ( $0.035A_{FB}^\tau$  and  $0.3\delta$ ) in the barrel (forward) regions, respectively.

The forward-backward charge asymmetries based on the thrust axis were calculated by the maximum likelihood method using the lowest order form for the angular distribution, and are given in Table 11 and shown in Figure 8 (b).

## 6.4 $l^+l^-$ Event Selection

An analysis of the channel  $Z^0 \rightarrow l^+l^-$  (where  $l = e, \mu, \tau$ ) has already been performed on the data taken during 1990 [1]. The work described here repeats that analysis on

Collision energy (GeV)		$A_{\text{FB}}^{\tau}$ (barrel)	$A_{\text{FB}}^{\tau}$ (forward)	Number of events (total)	$A_{\text{FB}}^{\tau}$ (total)
1990	1991				
88.221		$-0.30 \pm 0.18$		33	$-0.30 \pm 0.18$
	88.464	$-0.13 \pm 0.12$	$0.11 \pm 0.14$	108	$-0.070 \pm 0.090$
89.216		$0.00 \pm 0.13$		76	$0.00 \pm 0.13$
	89.455	$-0.073 \pm 0.085$	$-0.13 \pm 0.14$	192	$-0.120 \pm 0.072$
	90.209	$-0.218 \pm 0.064$	$0.013 \pm 0.092$	314	$-0.152 \pm 0.053$
90.212		$-0.12 \pm 0.08$		164	$-0.12 \pm 0.08$
	91.208	$0.000 \pm 0.024$	$0.027 \pm 0.037$	2438	$0.002 \pm 0.020$
91.213		$-0.014 \pm 0.026$		1738	$-0.014 \pm 0.026$
	91.238*	$0.049 \pm 0.019$	$0.023 \pm 0.031$	3821	$0.038 \pm 0.016$
	91.953	$0.067 \pm 0.052$	$0.178 \pm 0.070$	517	$0.101 \pm 0.042$
92.208		$0.04 \pm 0.08$		170	$0.04 \pm 0.08$
	92.953	$0.071 \pm 0.068$	$-0.06 \pm 0.11$	290	$0.031 \pm 0.059$
93.207		$0.03 \pm 0.12$		88	$0.03 \pm 0.12$
	93.702	$0.100 \pm 0.078$	$0.13 \pm 0.12$	237	$0.108 \pm 0.065$
94.201		$0.06 \pm 0.14$		76	$0.06 \pm 0.14$

Table 11: Measurement of the  $\tau^+\tau^-$  forward-backward asymmetry for different centre-of-mass energies. The results are corrected to the full solid angle. In the third and fourth columns are shown the values obtained with events selected in the barrel or forward region, respectively. The last column shows the global result. Statistical errors only are shown. The systematic errors at the peak are 0.003 for the 1991 data and 0.005 for the 1990 data. The 1991 pre-scan point is marked with a star.

data taken during 1991, incorporating several significant improvements. The presence of information from the three-layer microvertex detector led to much improved rejection of cosmic ray muons as a background, and the backgrounds coming from two-photon channels were reduced significantly by means of a cut on the transverse momentum, as well as being better understood.

The flavour independent analysis described here has several advantages over the conventional leptonic analyses. There is no need to separate the lepton families, and therefore the selection cuts may be looser, leading to a higher efficiency. The backgrounds are, as mentioned above, small and well-understood, and the analysis is based only on the charged particle detectors. This ensures that the event samples used in the flavour dependent and independent analyses are selected using significantly different criteria, and therefore this analysis provides a powerful consistency check.

The analysis can never truly be flavour independent, since the  $e^+e^-$ ,  $\mu^+\mu^-$  and  $\tau^+\tau^-$  fractions of the sample have to be determined in order to compute the  $e^+e^- \rightarrow e^+e^-$  t-channel contribution. The efficiencies of detection for the three families were computed, those for the electrons and muons directly from data using calorimeters to select independent data samples, and that for the taus from the Monte Carlo simulation. The trigger efficiency values used, which are also in principle, lepton type dependent, were those determined in the flavour dependent analyses described above. These trigger efficiencies are, however, all very close to 100 %. The event selection was performed as follows.

- The event had to have between 2 and 6 ‘good’ charged particles in the TPC, where ‘good’ implies that the particle had more than 0.2 GeV momentum and originated from within of  $\pm 4.5$  cm in  $z$  and 3.0 cm in  $r$  from the average interaction point.
- The analysis was restricted to the barrel region only; it was required that there were 2 or more ‘good’ charged particles having a polar angle between  $43^\circ$  and  $137^\circ$ .
- Dividing the event into two hemispheres by a plane perpendicular to the thrust axis, it was required that one hemisphere should contain one charged particle only and the other between 1 and 5 charged particles.
- For the group of 1 to 5 charged particles (hereafter called the ‘jet’ although no jet-finding algorithm is used) a resultant momentum was calculated, and it was required that this momentum vector should deviate by no more than  $20^\circ$  from the backwards projection of the direction of the isolated charged particle (they should have an acollinearity of less than  $20^\circ$  for any topology).
- No charged particle in the jet should be at an angle of more than  $30^\circ$  from the resultant.
- In order to eliminate beam-gas and two-photon events it was demanded that at least one charged particle in the event should have a momentum greater than 3.0 GeV.
- To reduce the background from two-photon events it was required that, if there were only two charged particles and both had a momentum less than 10 GeV, the total missing transverse momentum with respect to the beam direction should exceed 0.4 GeV.
- To reduce the background from cosmic ray muons, it was required that, if there were only two charged particles in the event, both particles should originate from a much smaller region around the average interaction point. For events where the microvertex detector information was present for both particles and there was a well reconstructed interaction point, this was 0.15 cm in  $r$  and 4.5 cm in  $z$ . If any of this information was missing (this was the case for approximately 15% of the data) the values were 1.5 cm and 4.5 cm, respectively.

These criteria resulted in the selection of 23,169 events for use in the cross section and asymmetry calculations, with a corresponding total integrated luminosity of  $10.7 \text{ pb}^{-1}$ . A re-analysis of the 1990 data was also made using the same selections as given above. Also the two-layer microvertex detector was included in the track-fit, leading to an improved rejection of cosmics and a better momentum resolution.

#### 6.4.1 Efficiencies

Events from the  $e^+e^-$  and  $\mu^+\mu^-$  channels are primarily of the  $1-1$  topology, hence the major loss for these channels was the failure to reconstruct one or both of the two particles and the subsequent rejection of the event in the selection criteria. Track loss can be divided into two sources — the passing of a particle through an insensitive region (‘crack’) of the TPC,  $(4.24 \pm 0.15)\%$ , and the failure to detect a particle in a ‘live’ region. The ‘live-space’ losses were  $(0.00 \pm 0.30)\%$  and  $(1.00 \pm 0.39)\%$  for muons and electrons respectively, giving final reconstruction efficiencies per track of  $(95.76 \pm 0.34)\%$  and  $(94.80 \pm 0.42)\%$  for muons and electrons, respectively.

It is difficult to select a sample of taus from the data in a manner independent of that described in this Section 6.4, as is required for a determination of the detection efficiency, so a sample of Monte Carlo events generated using KORALZ [11] was treated with exactly the same analysis procedure as the real data. The efficiency was found to be  $(55.51 \pm 0.51)\%$ , which corresponds to an efficiency of  $(83.30 \pm 0.77)\%$  for  $\tau^+\tau^-$  events

in the barrel region. Both these figures include a correction of  $(0.65 \pm 0.25)\%$  to match the differences in the losses in the TPC cracks between Monte Carlo simulation and data.

A correction must also be applied for the trigger efficiencies. The correction factor was the average value for the individual lepton channels, weighted by the estimated number of events from that channel in the sample.

### 6.4.2 Backgrounds

There are several backgrounds to the leptonic channels which must be considered. The three primary ones are those arising from cosmic ray muons, two-photon events and  $Z^0$  events with hadronic final states. The background from cosmic rays was calculated using the distribution of impact parameters within the data, and extrapolating into the selected region. It was found to be 98 events with two charged particles and 82 events with three. The relative background from events with three detected charged particles was larger because of the less stringent vertex selection criteria for this topology. The cosmic background events were distributed over the energy range according to the total integrated luminosity recorded at each point, as an approximation to the time spent taking data at each energy. The final estimate of the background on the peak was 0.61% with an error of 0.04%.

The two-photon background was studied using the generator described in ref. [13]. The contributions from the  $e^+e^-e^+e^-$ ,  $e^+e^-\mu^+\mu^-$ ,  $e^+e^-\tau^+\tau^-$ ,  $e^+e^-hadrons$  channels were all evaluated separately by generating 50,000 to 100,000 events of each sort. It was found that the initial demands on the momentum reduced the background considerably, and then that the missing transverse momentum cut was extremely powerful in rejecting the  $e^+e^-e^+e^-$  and  $e^+e^-\mu^+\mu^-$  cases, whilst the isolation angle cuts (those on opening angle and acollinearity) were effective against the  $e^+e^-\tau^+\tau^-$  and  $e^+e^-hadrons$  states. The results were investigated for model dependence and stability to the simulated beam energy. The final result is a total two-photon background cross section of  $5.8 \pm 0.3$  pb. The error represents a combination of the statistical error on the number of events passing the cuts and the estimated error from the generator for each contribution. This background is non-resonant and is to be subtracted from the final cross sections after they have been corrected for efficiencies and backgrounds, but before they are scaled up to  $4\pi$  solid angle.

The hadronic background was calculated from a sample of 152,000 Monte Carlo events simulating the 1991 running conditions, of which 1749 had 8 or fewer charged particles. Of this sample only 16 passed the final cuts (the isolation angle cut being the most effective). This number, as a fraction of the number of initial hadrons, was then scaled using the hadron cross section at each energy to produce a resonant background of  $(0.12 \pm 0.03)\%$  where the error comes from the low statistics and uncertainty in the accuracy of the Monte Carlo simulation at these low multiplicities.

### 6.4.3 Cross Section

The cross section was calculated for each of the energies at which LEP produced collisions in 1991, with the point nearest to the  $Z^0$  mass split into two for data collected in the early part of the year, and that collected during the line-scan. The number of events selected at each point was modified by corrections for the backgrounds given above, and corrected by a factor of 1.001 for the trigger efficiency. The number of electrons within the sample was then determined using the individual selection efficiencies, and hence the contribution of  $e^+e^-$  t-channel was computed and subtracted. The remaining total was

then corrected using the selection efficiencies and geometrical correction to give a cross section over the full solid angle.

The values thus obtained are given, reduced to one lepton generation, as a function of centre-of-mass energy in the third column of Table 12. These cross sections have not been corrected for the effects of the cuts on momenta and acollinearity angle. Also given are the results from the analysis of the 1990 data.

The  $e^+e^- \rightarrow e^+e^-$  t-channel contribution was subtracted using the programs ALIBABA [14], and 40THIEVES [19]. This was calculated in a similar way to that discussed in Section 6.1.3. Taking into account the fraction of electron events in the selected sample, the systematic uncertainties are equivalent to a 0.12% error in the cross section. The overall systematic error for the 1991 (1990) data is 0.4% (0.6%), excluding the error from the luminosity measurements.

Collision energy (GeV)		Cross sections ( $4\pi$ ) (nb)	Integ. L. (nb <sup>-1</sup> )	Number of events
1990	1991			
88.223		$0.202 \pm 0.015$	294	171
	88.464	$0.229 \pm 0.011$	712	440
89.221		$0.399 \pm 0.020$	423	406
	89.457	$0.469 \pm 0.018$	635	683
	90.211	$0.834 \pm 0.025$	638	1099
90.223		$0.922 \pm 0.034$	384	728
	91.208	$1.441 \pm 0.018$	2462	6672
91.225		$1.433 \pm 0.017$	2706	7185
	91.239*	$1.436 \pm 0.014$	4236	11483
	91.953	$1.192 \pm 0.031$	666	1440
92.219		$1.049 \pm 0.037$	424	795
	92.952	$0.675 \pm 0.024$	634	763
93.223		$0.555 \pm 0.027$	432	433
	93.702	$0.484 \pm 0.020$	681	589
94.218		$0.345 \pm 0.020$	470	304

Table 12: The number of selected events, integrated luminosities and cross sections for  $e^+e^- \rightarrow l^+l^-$  for different centre-of-mass energies measured in 1990 and 1991. The 1991 pre-scan point is marked with a star. The results are for one generation and corrected for  $e^+e^-$  t-channel subtraction. They are corrected to the full solid angle, but not for the cuts on momenta and acollinearity. The uncertainties quoted are statistical. The total systematic error on the cross section data for 1991 is 0.4%, in addition to the error on the luminosity. The uncertainties quoted for 1990 are again statistical only. The total systematic error on the cross section is 0.6%, in addition to the uncertainty in the luminosity.

#### 6.4.4 Forward - Backward Asymmetry

In computing the forward-backward asymmetry, only those events having a 1 – 1 topology in which the two tracks were oppositely charged were retained, leading to a final sample of 18,074 events. Of the 160 events having both leptons identified with the same charge in the tracking detectors, 74 could have the charge ambiguity resolved by

including information about the positioning of energy deposits in the HPC associated with the track, and were used in the asymmetry measurement. The fraction of events giving rise to just two charged particles was determined for each family using the simulation, and the efficiencies adjusted accordingly when calculating the fraction of electrons within the final sample. A counting method was used to compute the asymmetry over the barrel region and corrections were applied for the cosmic ray and two-photon backgrounds. The asymmetry due to the  $e^+e^- \rightarrow e^+e^-$  t-channel was calculated using both ALIBABA [14] and 40THIEVES [19] as in Section 6.4.3 above, and this was scaled by the electron fraction of the sample and removed. The results were finally corrected to the whole solid angle range.

In Table 13 the values of the charge asymmetry are given after t-channel subtraction and correction to the full solid angle. The main source of systematic error comes from possible misidentification of the charge. This was estimated to be 0.0020. Other systematics which must be considered are the uncertainty on the t-channel asymmetry and the calculated electron fraction, which together contributed 0.0016, making a total systematic error of 0.0025. Also given in Table 13 are the results for the 1990 data. The total systematic error for these data is 0.005.

Collision energy (GeV)		Number of events	$A_{\text{FB}}^l$
1990	1991		
88.223		157	$-0.273 \pm 0.093$
	88.464	329	$-0.264 \pm 0.064$
89.221		304	$-0.303 \pm 0.067$
	89.457	520	$-0.174 \pm 0.052$
	90.211	861	$-0.089 \pm 0.040$
90.223		565	$-0.150 \pm 0.049$
	91.208	5237	$0.015 \pm 0.016$
91.225		5661	$-0.010 \pm 0.016$
	91.239*	8939	$0.025 \pm 0.013$
	91.953	1111	$0.085 \pm 0.035$
92.219		510	$-0.016 \pm 0.052$
	92.952	607	$0.157 \pm 0.048$
93.223		330	$0.142 \pm 0.064$
	93.702	458	$0.079 \pm 0.055$
94.218		230	$0.235 \pm 0.076$

Table 13: Results of measurements of the  $l^+l^-$  forward-backward asymmetry at different centre-of-mass energies for 1990 and 1991 data. The 1991 pre-scan point is marked with a star. The results are for one generation and corrected for t-channel subtraction. They are corrected to the full solid angle, but not for the cuts on momenta and acollinearity. The errors are statistical only; the systematic error on these points is 0.005 for the 1990 data and 0.0025 for the 1991 data.

## 6.5 Comparison with Lepton Flavour Identified Results

As discussed above, one of the advantages of the lepton flavour independent analysis is that it has somewhat different systematic errors to the flavour identified channels and



so the results serve as a cross-check. In order to make such a cross-check, all the cross section results for 1991 data were corrected (using ZFITTER[16]) so that they correspond to a  $4\pi$  detector with no cut applied. The weighted mean of the lepton identified results was computed as a function of centre-of-mass energy. The ratio of this mean value to the measured cross section for  $e^+e^- \rightarrow l^+l^-$  was then computed. In the computation of the error on this ratio the systematic errors on the various channels, as well as the statistical error due to the incomplete overlap of the different channels, were taken into account. The latter arises because the different analyses have somewhat different polar angle ranges and that the runs selected have different requirements on which sub-detectors should be fully functional. The cross sections for the lepton flavour independent and the weighted average of the flavour dependent results, all corrected to  $4\pi$  acceptance, are shown in Figure 9, together with the values of the ratios of these cross sections. The average value of these ratios over all energies, which should be unity, was found to be  $0.999 \pm 0.005$ . Given the different angular ranges of the analysed data, and the different correction factors involved in the different analyses, this agreement shows that the cross-check supports the validity of the lepton identified data.

A comparison was also made of the results on the forward-backward asymmetry. Again all the results were corrected for the cuts, where appropriate, so that they correspond to a  $4\pi$  angular range with no cut on momenta or acollinearity. The differences between the weighted mean of the lepton flavour identified samples and the lepton flavour independent samples were then computed. Again, the systematic error, and the statistical error from the non-complete overlap of the samples used, were taken into account when computing the error on the difference. Averaged over all values of the centre-of-mass energies, the difference in the forward-backward asymmetry between the lepton flavour identified and independent samples is  $(-0.010 \pm 0.009)$ , again showing the consistency of the measurements.

## 7 $Z^0$ Parameters and Electroweak Couplings

Fits to the hadronic cross sections and the flavour separated leptonic cross sections and asymmetries have been made using the program ZFITTER (version 4.6). The theoretical formalism of the ZFITTER calculations allows an almost model independent interpretation of the observed quantities, taking into account the most up-to-date knowledge of initial and final state QED effects, electroweak and QCD corrections. A previous version of ZFITTER (version 4.5) is described in detail in ref. [16]. With respect to the formulae used for the analysis of DELPHI 1990 data [1](i.e. ZFITTER version 3.05), the program has been updated with a better understanding of QCD corrections and terms dependent on the top mass  $m_t$ . In addition the present version 4.6 accounts also for light fermion pair production [20], for corrections of order  $(G_F m_t^2)^2$ , where  $G_F$  is the Fermi coupling constant, for arbitrary Higgs mass  $m_H$  [21] and for the most recent treatment of the QCD corrections [22] for the  $b\bar{b}$  channel.

Only the light fermion pair production correction is numerically important for the model independent fits. Taking account of this correction changes the mass of the  $Z^0$ ,  $M_Z$ , and its width,  $\Gamma_Z$ , by about 1 MeV and 2 MeV, respectively. The rest of the corrections are to a great extent absorbed in the definitions of the partial widths and/or couplings and are essential only for further interpretation of the model independent fit results in the framework of the Standard Model (i.e. for the determination of  $m_t$  and the strong coupling constant  $\alpha_s$ ). Before QED radiative corrections the cross section for

$e^+e^- \rightarrow \text{hadrons}$  can be written as

$$\sigma(s) = \sigma_0 \frac{s\Gamma_Z^2}{(s - M_Z^2)^2 + (s^2/M_Z^2)\Gamma_Z^2}. \quad (2)$$

Small corrections arising from  $\gamma$  exchange and  $\gamma$ - $Z$  interference were calculated within the framework of the Standard Model. The hadronic pole cross section,  $\sigma_0$ , can be expressed in terms of the hadronic and electronic partial widths,  $\Gamma_{\text{had}}$  and  $\Gamma_e$ , as

$$\sigma_0 = \frac{12\pi\Gamma_e\Gamma_{\text{had}}}{M_Z^2\Gamma_Z^2}, \quad (3)$$

with similar expressions for the leptonic cross sections. The parameters  $R_f$ , for lepton species  $f$ , are defined as

$$R_f = \frac{\Gamma_{\text{had}}}{\Gamma_f}. \quad (4)$$

The leptonic partial widths  $\Gamma_f$  can be written in terms of effective vector and axial-vector couplings,  $g_{V_f}$  and  $g_{A_f}$ , as

$$\Gamma_f = \frac{G_F M_Z^3}{6\pi\sqrt{2}}(g_{V_f}^2 + g_{A_f}^2)\left(1 + \frac{3\alpha}{4\pi}\right), \quad (5)$$

where  $\alpha$  is the fine structure constant of QED, and the last factor accounts for final state radiation.

In order to fit the hadronic and leptonic cross sections and leptonic forward-backward asymmetries, allowing independent couplings for each lepton species, the parameters  $M_Z, \Gamma_Z, \sigma_0, R_f$  and  $A_{\text{FB}}^{\circ f}$  are chosen, where

$$A_{\text{FB}}^{\circ f} = 3 \frac{g_{V_e}g_{A_e}}{(g_{V_e}^2 + g_{A_e}^2)} \frac{g_{V_f}g_{A_f}}{(g_{V_f}^2 + g_{A_f}^2)}. \quad (6)$$

This set of parameters was chosen because they have minimal correlations between them and are therefore to be preferred if the combining of data from the different LEP experiments is envisaged. To lowest order the forward-backward asymmetry in the reaction  $e^+e^- \rightarrow f^+f^-$  at  $\sqrt{s} = M_Z$  is given by eq.(6). Away from the peak the asymmetry varies rapidly with energy and is mainly proportional to  $g_{A_e}g_{A_f}$ .

A  $\chi^2$  minimization procedure was adopted for the fitting of the theoretical expressions to the measured lineshapes and asymmetries, including a full covariance matrix treatment of the errors. Full account was taken of the LEP energy uncertainties and their point-to-point correlations. The overall energy scale of the 1990 data was assigned an uncertainty of 26 MeV. The 9-parameter fit yields the following results :

$$\begin{aligned} M_Z &= 91.187 \pm 0.009 \text{ GeV} \\ \Gamma_Z &= 2.486 \pm 0.012 \text{ GeV} \\ \sigma_0 &= 40.90 \pm 0.28 \text{ nb} \\ R_e &= 20.82 \pm 0.28 \\ R_\mu &= 20.75 \pm 0.22 \\ R_\tau &= 20.83 \pm 0.28 \\ A_{\text{FB}}^{\circ e} &= 0.007 \pm 0.015 \\ A_{\text{FB}}^{\circ \mu} &= 0.015 \pm 0.008 \\ A_{\text{FB}}^{\circ \tau} &= 0.027 \pm 0.010 \\ \chi^2/DF &= 100/97. \end{aligned} \quad (7)$$

	$\Gamma_Z$	$\sigma_0$	$R_e$	$R_\mu$	$R_\tau$	$A_{\text{FB}}^{\circ e}$	$A_{\text{FB}}^{\circ \mu}$	$A_{\text{FB}}^{\circ \tau}$
$M_Z$	0.00	0.02	0.01	0.00	0.00	0.02	0.04	0.04
$\Gamma_Z$	1.00	-0.20	0.00	0.00	0.00	0.00	-0.01	0.00
$\sigma_0$		1.00	0.07	0.10	0.08	0.00	0.00	0.00
$R_e$			1.00	0.05	0.04	0.00	0.00	0.00
$R_\mu$				1.00	0.05	0.00	0.02	0.00
$R_\tau$					1.00	0.00	0.00	0.02
$A_{\text{FB}}^{\circ e}$						1.00	0.00	0.00
$A_{\text{FB}}^{\circ \mu}$							1.00	0.01

Table 14: The correlation matrix for the parameters of the 9-parameter fit.

The correlation matrix for the parameters of the 9-parameter fit is given in Table 14.

The contour plot of  $A_{\text{FB}}^{\circ f}$  versus  $R_f$  for each lepton species is shown in Figure 10. It can be seen that there is excellent agreement with lepton universality. A 5-parameter fit assuming flavour independence<sup>†</sup> of the couplings yields the following parameters:

$$\begin{aligned}
M_Z &= 91.187 \pm 0.009 \text{ GeV} \\
\Gamma_Z &= 2.486 \pm 0.012 \text{ GeV} \\
\sigma_0 &= 40.90 \pm 0.28 \text{ nb} \\
R_l &= 20.78 \pm 0.15 \\
A_{\text{FB}}^{\circ} &= 0.017 \pm 0.006 \\
\chi^2/DF &= 102/101,
\end{aligned} \tag{8}$$

where  $R_l$  and  $A_{\text{FB}}^{\circ}$  are defined analogously to eqs.(4) and (6), respectively, but assuming lepton universality. The correlation matrix of the parameters of the 5-parameter fit is given in Table 15.

In Figure 11 the results of the 5-parameter fit are shown in terms of allowed contours in the  $\sigma_0 - \Gamma_Z$  plane.

Alternatively the results of the preceding fits can be expressed in terms of the following derived parameters:

$$\begin{aligned}
\Gamma_e &= 82.93 \pm 0.70 \text{ MeV} \\
\Gamma_\mu &= 83.20 \pm 1.11 \text{ MeV} \\
\Gamma_\tau &= 82.89 \pm 1.31 \text{ MeV} \\
\Gamma_l &= 83.01 \pm 0.52 \text{ MeV} \\
g_{V_l}^2 &= (1.47 \pm 0.51) \times 10^{-3} \\
g_{A_l}^2 &= 0.2483 \pm 0.0016 \\
\Gamma_{\text{inv}} &= 512 \pm 10 \text{ MeV} \\
\Gamma_{\text{had}} &= 1.725 \pm 0.012 \text{ GeV},
\end{aligned} \tag{9}$$

where  $\Gamma_{\text{inv}}$  is the partial width for  $Z^0$  decays into invisible final states and  $\Gamma_l, g_{V_l}, g_{A_l}, \Gamma_{\text{inv}}$  and  $\Gamma_{\text{had}}$  are defined assuming lepton universality. If the effective weak mixing angle is defined by the relation

$$g_{V_l}/g_{A_l} = (1 - 4 \sin^2 \theta_{\text{eff}}^{\text{lept}}), \tag{10}$$

<sup>†</sup>In the present analysis  $R_l$  (and similarly  $\Gamma_l$ ) is defined for the  $Z^0$  decay into a pair of massless charged leptons, and is treated consistently throughout. The value using other definitions, can be obtained from the results of the 9-parameter fit.

where  $g_{V_l}/g_{A_l}$  is derived from the leptonic forward-backward asymmetries, then these results yield

$$\sin^2\theta_{eff}^{lept} = 0.2308 \pm 0.0033. \quad (11)$$

The results of the 5-parameter and 9-parameter fits to the DELPHI data are in good agreement with those published by the other LEP collaborations [23–25].

	$\Gamma_Z$	$\sigma_0$	$R_l$	$A_{FB}^0$
$M_Z$	0.00	0.02	0.01	0.06
$\Gamma_Z$	1.00	-0.20	0.00	-0.01
$\sigma_0$		1.00	0.14	0.00
$R_l$			1.00	0.01

Table 15: The correlation matrix for the parameters of the 5-parameter fit.

## 8 Interpretation of the Results within the Standard Model

From the values of  $\sigma_0$  and  $R_l$  and using the expression

$$\Gamma_{inv}/\Gamma_l = \sqrt{\frac{12\pi R_l}{M_Z^2 \sigma_0}} - R_l - 3, \quad (12)$$

the result

$$\Gamma_{inv}/\Gamma_l = 6.17 \pm 0.12 \quad (13)$$

is obtained. Hence, assuming the Minimal Standard Model (MSM) value for  $\Gamma_\nu/\Gamma_l$ ,

$$\Gamma_\nu/\Gamma_l = 1.992 \pm 0.003, \quad (14)$$

where  $\Gamma_\nu$  is the  $Z^0$  partial width into a  $\nu\bar{\nu}$  pair, the number of light neutrino species can be deduced:

$$N_\nu = 3.10 \pm 0.06. \quad (15)$$

If a Standard Model fit is carried out, leaving the number of neutrino species free, but using as a constraint the value of the strong coupling constant  $\alpha_s$  recently determined by the DELPHI experiment [26],

$$\alpha_s = 0.123 \pm 0.005, \quad (16)$$

the number of light neutrino species is found to be :

$$N_\nu = 3.08 \pm 0.05. \quad (17)$$

If the number of neutrino species is fixed to be three, but  $\alpha_s$  is left unconstrained, then the fit yields the value:

$$\alpha_s = 0.136 \pm 0.018. \quad (18)$$

The consistency of these results with the MSM can be seen in Figures 10 and 11 where the predictions for a range of values of  $m_t$ ,  $\alpha_s$  and  $m_H$  are shown.

A Standard Model fit, assuming three neutrino species, to the cross section and asymmetry data using the value of  $\alpha_s$  from eq.(16) as a constraint, yields the following value for the top quark mass:

$$m_t = 115_{-82}^{+52}(\text{expt.})_{-24}^{+23}(\text{Higgs}) \text{ GeV}, \quad (19)$$

where (*Higgs*) represents the variation due to Higgs boson masses in the range 60 to 1000 GeV, with central value 300 GeV. The lower experimental limit is badly determined and is in any case excluded by searches at hadron colliders [27].

This value of  $m_t$  corresponds to:

$$\sin^2\theta_{eff}^{lept} = 0.2339 \pm 0.0015(\text{expt.})_{-0.0004}^{+0.0001}(\text{Higgs}). \quad (20)$$

## 9 Fits in Terms of the Variables S and T

The standard variables used in the analysis of LEP data ( $\Gamma_Z, \Gamma_{had}, \Gamma_l$ , etc.) can be expressed in terms of variables S and T [28,29] which parameterize loop effects, through the relationships

$$\begin{aligned} \rho &= 1 + \alpha(M_Z)T \\ \Delta\hat{r} &= \Delta\hat{r}_{\text{MSM}} + \frac{\alpha(M_Z)S}{4\hat{s}_0^2\hat{c}_0^2} - \alpha(M_Z)T, \end{aligned} \quad (21)$$

where

$$\begin{aligned} \Delta\hat{r}_{\text{MSM}} &= 1 - \frac{\pi\alpha}{\sqrt{2}G_F M_Z^2 \hat{s}_0^2 \hat{c}_0^2} \\ \hat{s}_0^2 &= \sin^2\theta_{\overline{\text{MS}}}(M_Z^2) \\ \hat{c}_0^2 &= 1 - \hat{s}_0^2. \end{aligned} \quad (22)$$

The weak mixing angle  $\theta_{\overline{\text{MS}}}$  is defined in the  $\overline{\text{MS}}$  renormalization scheme (see refs. [28,29]). The values  $S = T = 0$  are defined to correspond to  $m_t = 140$  GeV,  $m_H = 300$  GeV and  $\alpha_s = 0.123$ . The results of the fit are shown in Figure 12. The central values are:

$$\begin{aligned} S &= -1.33 \pm 1.19 \\ T &= -0.72 \pm 0.71. \end{aligned} \quad (23)$$

In an alternative approach [30] the effects of new physics in the gauge boson vacuum polarization diagrams can be expressed in terms of the parameters  $\epsilon_1$ ,  $\epsilon_2$  and  $\epsilon_3$ . The LEP data do not constrain the parameter  $\epsilon_2$ . The parameters  $\epsilon_1$  and  $\epsilon_3$  are uniquely defined from the measured values of the leptonic width  $\Gamma_l$  and forward-backward asymmetry  $A_{\text{FB}}^o$  at  $\sqrt{s} = M_Z$ . Using the values of  $\Gamma_l$  and  $A_{\text{FB}}^o$  given in Section 7, the following values are obtained:

$$\begin{aligned} \epsilon_1 &= -0.0049 \pm 0.0066 \\ \epsilon_3 &= -0.0044 \pm 0.0106. \end{aligned} \quad (24)$$

These parameters have the advantage that their values do not depend on the masses of the top-quark and Higgs boson, or on  $\alpha_s$ . However, in the interpretation of these parameters to investigate, for example, physics beyond the MSM, these quantities must of course be specified.

## 10 Lower Bounds on New Particle Masses

The absence of any significant departure of the observed values of  $\Gamma_Z$  and  $\Gamma_{\text{inv}}$  from the MSM predictions has been converted into lower mass bounds of new particles connected with physics beyond the MSM.

The approach described in ref. [1] was repeated in order to determine 95% confidence level upper limits of the potential extra total and invisible widths,  $\Gamma_Z^{\text{new}}$  and  $\Gamma_{\text{inv}}^{\text{new}}$ , associated to these new particles. The values found are:

$$\begin{aligned}\Gamma_Z^{\text{new}} &< 27 \text{ MeV} \\ \Gamma_{\text{inv}}^{\text{new}} &< 26 \text{ MeV.}\end{aligned}\tag{25}$$

With these values the lower mass bounds published in ref. [1] remain essentially unchanged.

## 11 Summary

During 1990 and 1991 approximately 450,000  $Z^0$  decays into hadrons and charged leptons were observed in the DELPHI detector. The increased event statistics coupled with improvements to the detector and the analysis techniques have allowed the hadronic and leptonic cross sections and the leptonic forward-backward asymmetries to be measured with high precision. The 1990 data have been re-evaluated with improved luminosity measurements. For the 1991 data, the use of the high rate luminosity monitor VSAT has significantly reduced the statistical errors. Using the accurate determinations of the LEP energy, model independent fits to the data yield significantly improved determinations of the  $Z^0$  resonance parameters. A flavour independent analysis gives leptonic cross sections and asymmetries compatible with those measured in the individual channels. Lepton universality of the  $Z^0$  partial widths is confirmed at the 2% level. Assuming lepton universality the following parameters are obtained:

$$\begin{aligned}M_Z &= 91.187 \pm 0.009 \text{ GeV} \\ \Gamma_Z &= 2.486 \pm 0.012 \text{ GeV} \\ \sigma_0 &= 40.90 \pm 0.28 \text{ nb} \\ R_l &= 20.78 \pm 0.15 \\ A_{\text{FB}}^o &= 0.017 \pm 0.006.\end{aligned}$$

From the values of  $\sigma_0$  and  $R_l$ , the number of light neutrino species has been determined to be

$$N_\nu = 3.10 \pm 0.06$$

or, if DELPHI measurements of the strong coupling constant  $\alpha_s$  [26] are used as a constraint,

$$N_\nu = 3.08 \pm 0.05.$$

All cross sections and asymmetries measured are consistent with the Standard Model expectations. A fit within the context of that model, using also the DELPHI determination of  $\alpha_s$  [26], constrains the value of the top mass to be

$$m_t = 115_{-82}^{+52}(\text{expt.})_{-24}^{+23}(\text{Higgs}) \text{ GeV},$$

corresponding to a value of the weak mixing angle

$$\sin^2\theta_{eff}^{lept} = 0.2339 \pm 0.0015 (expt.)_{-0.0004}^{+0.0001} (Higgs).$$

Fits to the data have also been performed using variables which parameterize electroweak loop effects, and which are sensitive to physics beyond the Minimal Standard Model.

## Acknowledgements

We are greatly indebted to our technical collaborators and to the funding agencies for their support in building and operating the DELPHI detector, and to the members of the CERN-SL Division for the excellent performance of the LEP collider.

## References

- [1] DELPHI Collaboration, P. Abreu et al., Nucl. Phys. **B367** (1991) 511.
- [2] L. Arnaudon et al., Phys. Lett. **B284** (1992) 431 .
- [3] The Working Group on LEP Energy and the LEP Collaborations ALEPH, DELPHI, L3 and OPAL, Phys. Lett. **B307** (1993) 187.
- [4] DELPHI Collaboration, P. Aarnio et al. , Nucl. Instr. & Meth. **A303** (1991) 233.
- [5] N. Bingefors et al., Nucl. Instr. & Meth. **A328** (1993) 447.
- [6] DELPHI Collaboration, “High precision relative luminosity measurement with a Very Small Angle Tagger (VSAT) in DELPHI”, DELPHI Note 92-77 (1992), unpublished.
- [7] S. Jadach et al., Comput. Phys. Commun. **70** (1992) 305.
- [8] F.A. Berends, W. Hollik and R.Kleiss, Nucl. Phys. **B304** (1988) 712.
- [9] W. Beenaker and B. Pietrzyk, Phys. Lett. **B296** (1992) 241.
- [10] J. Cuevas et al., Nucl. Instr. & Meth. **A274** (1989) 459.
- [11] S. Jadach, B.F.L. Ward, Z. Was, Comput. Phys. Commun., 66 (1991) 276.
- [12] J.E. Campagne and R. Zitoun, Z. Phys. **C43** (1989) 469.
- [13] S. Nova, A. Olchevski and T. Todorov, “Monte Carlo event generator for two photon processes”, DELPHI Note 90-35 (1990), unpublished.
- [14] W.J.P. Beenakker, F.A. Berends and S.C. van der Marck, Nucl. Phys. **B349** (1991) 323.
- [15] G. Montagna et al., Nucl. Phys. **B401** (1993) 3, and Comput. Phys. Commun. **76** (1993) 328.
- [16] D. Bardin et al., “ZFITTER: An Analytical Program for Fermion Pair Production in  $e^+e^-$  Annihilation”, preprint CERN-TH 6443/92 (1992) and references therein.
- [17] N. Crosland, G. Wilkinson and P. Kluit, “EMMASS muon identification within DELPHI”, DELPHI Note 92-17 (1992), unpublished.
- [18] DELPHI collaboration, “DELPHI Event generation and detector simulation - User guide”, DELPHI Note 89-67 (1989), unpublished.
- [19] M. Cacciari et al., Phys. Lett. **B268** (1991) 44.
- [20] B. Kniehl et al., Phys.Lett. **B209** (1988) 337; S. Jadach, M. Skrzypec and M. Martinez, Phys. Lett. **B280** (1992) 129.
- [21] R. Barbieri et al., “Two loop heavy top effects in the Standard Model”, preprint CERN-TH 6713/92 (1992).
- [22] K. G. Chetyrkin et al., Phys.Lett. **B282** (1992) 221; K. G. Chetyrkin et al., Phys.Lett. **B248** (1990) 359.
- [23] ALEPH Collaboration, D. Buskulic et al., Z. Phys. **C60** (1993) 71.
- [24] L3 Collaboration, O. Adriani et al., “Results from the L3 Experiment at LEP”, preprint CERN-PPE/93-31, Physics Reports to be published.
- [25] OPAL Collaboration, P.D. Acton et al., Z. Phys. **C58** (1993) 219.
- [26] DELPHI Collaboration, P. Abreu et al., Z. Phys. **C59** (1992) 21.
- [27] CDF Collaboration, F. Abe et al., Phys. Rev. Lett. **68** (1992) 447.
- [28] W.J. Marciano and J.L. Rosner, Phys. Rev. Lett. **65** (1990) 2963.
- [29] M.E. Peskin and T. Takeuchi, Phys. Rev. Lett. **65**, (1991) 964.
- [30] G. Altarelli and R. Barbieri, Phys. Lett. **B253** (1991) 161; G. Altarelli, R. Barbieri and S. Jadach, Nucl. Phys. **B369** (1992) 3; G. Altarelli, R. Barbieri and F. Caravaglios, Nucl. Phys. **B405** (1993) 3.



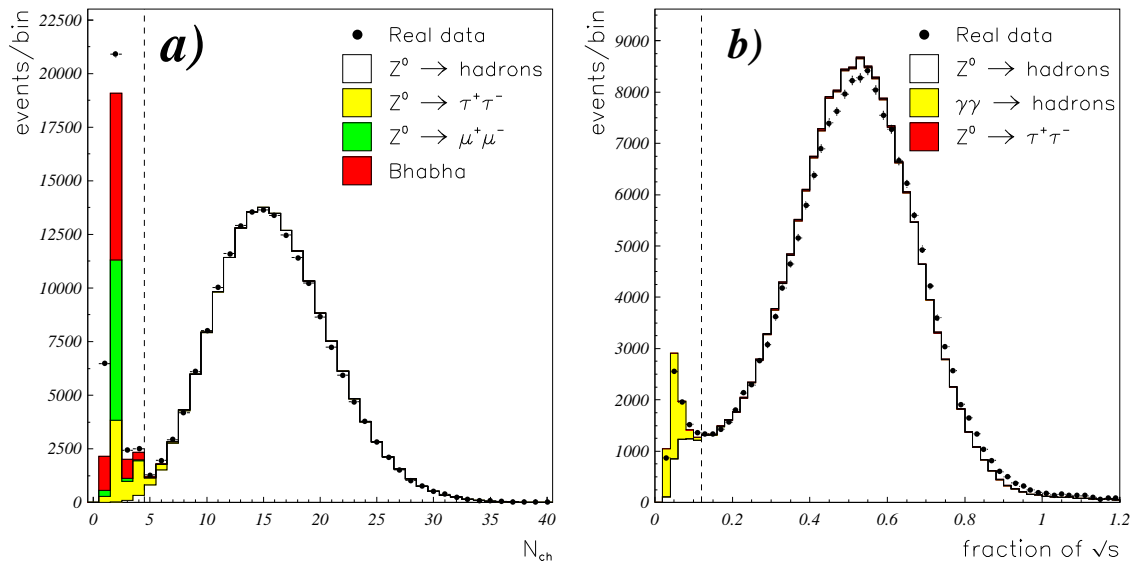


Figure 1: The distributions of the charged multiplicity  $N_{ch}$  (a) and charged energy  $E_{ch}$  normalized to the collision energy (b). The points show the real data distributions. The unshaded area under the full line corresponds to the simulated  $q\bar{q}$  sample. The shaded areas show the distributions of the different backgrounds. The same data and Monte Carlo samples are used in both plots. In (a) the  $E_{ch}$  cut and in (b) the  $N_{ch}$  cut have been applied.

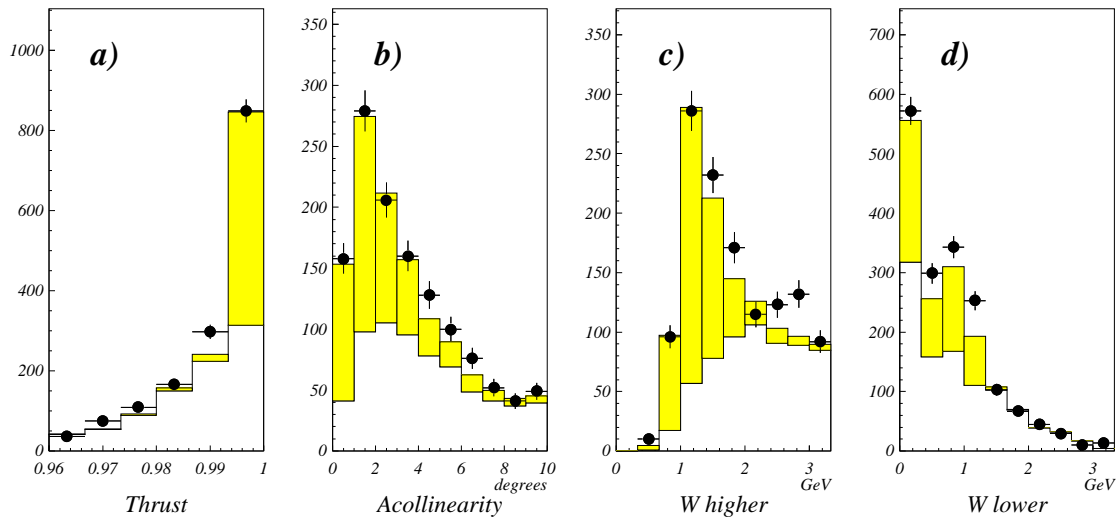


Figure 2: The distributions of the thrust (a), of the acollinearity angle (b) and of the higher ( $W_{higher}$ ) (c) and lower ( $W_{lower}$ ) (d) invariant mass per hemisphere, for selected events with a charged multiplicity equal to 5 or 6. The points correspond to the real data, the unshaded areas to the simulated  $q\bar{q}$  sample and the shaded areas to the  $\tau^+\tau^-$  Monte Carlo simulation.

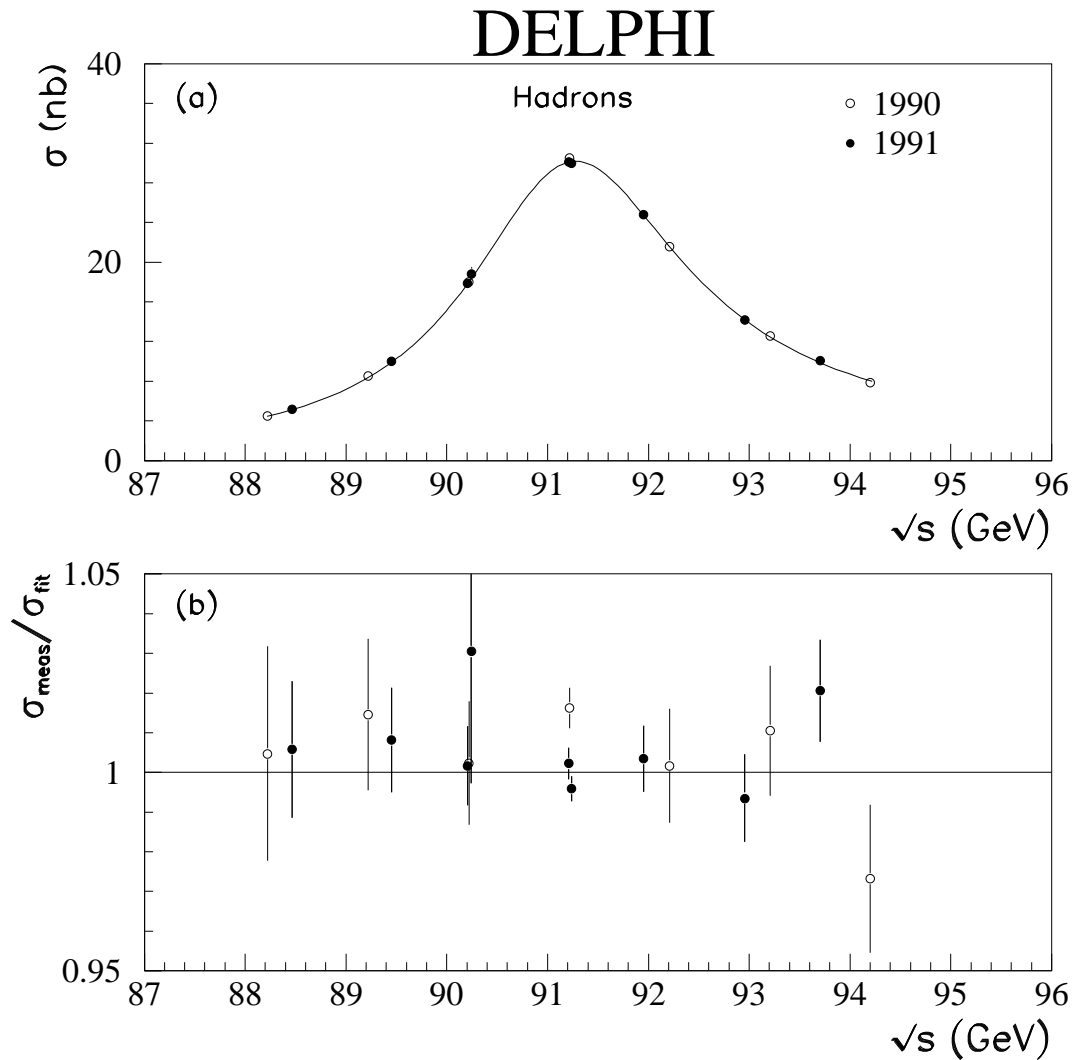


Figure 3: Hadronic cross sections from 1990 and 1991 data. The errors shown are statistical only. The uncorrelated systematic error between the 1990 and 1991 results amounts to 0.6%. In (a) the data are shown together with the result of the 5-parameter fit described in Section 7. Plot (b) shows the ratio of the measurements to the best fit values.

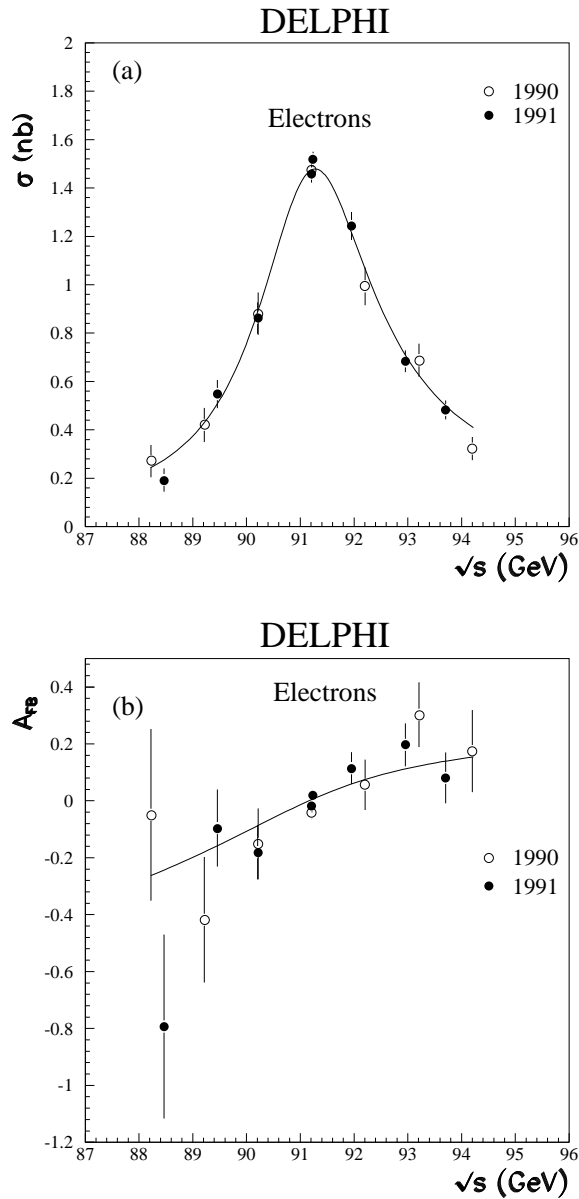


Figure 4: Cross sections and forward-backward charge asymmetries in the  $e^+e^-$  channel  
 (a) Cross sections (s-channel only), extrapolated to the full solid angle and corrected for the acollinearity and momentum cuts.

(b) Forward-backward charge asymmetries (s-channel only) within the angular range  $44^\circ < \theta < 136^\circ$ .

The curves are the results of the 5-parameter fit described in Section 7.

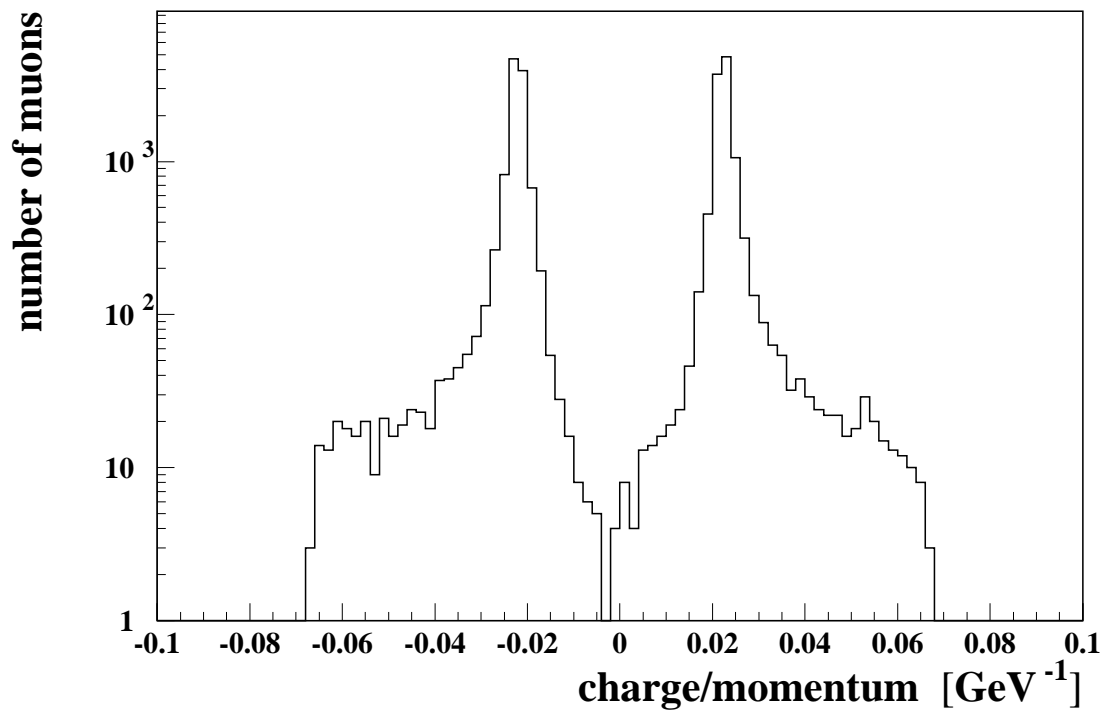


Figure 5: The distribution of the electric charge multiplied by the inverse momentum for reconstructed tracks in the polar angle range  $11^\circ < \theta < 169^\circ$  and used in the  $e^+e^- \rightarrow \mu^+\mu^-$  analysis of the forward-backward asymmetry.

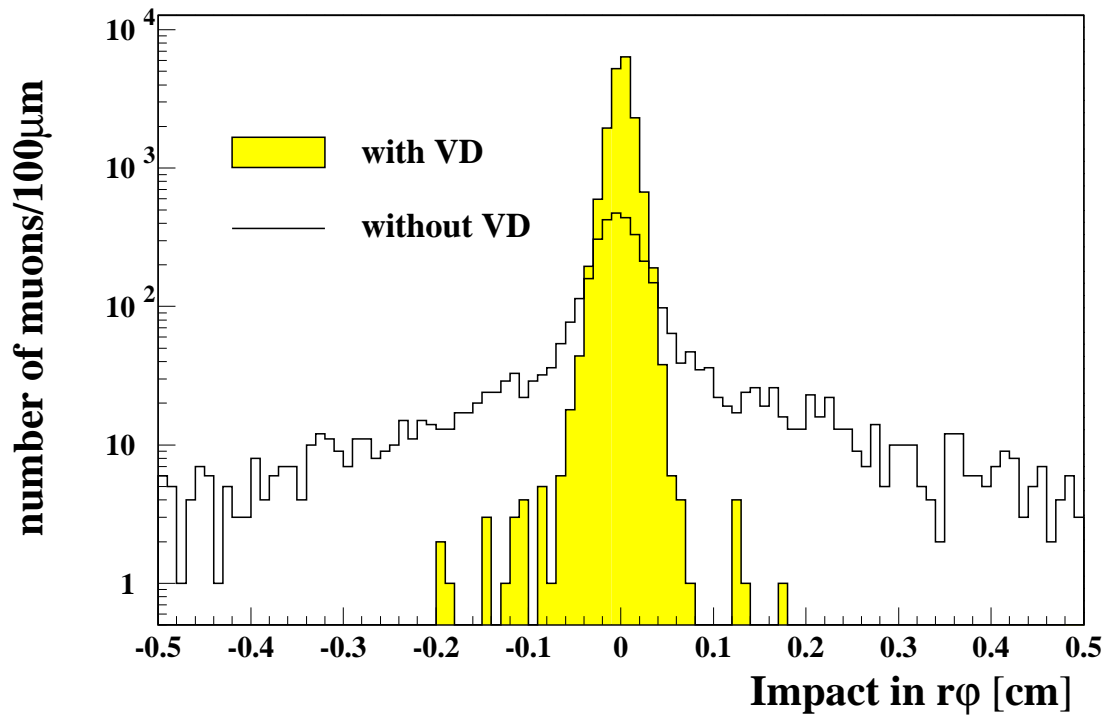


Figure 6: The distribution of the impact parameter, which is defined as the distance of closest approach to the average interaction point position in the transverse plane, for  $\mu^+\mu^-$  events. The shaded distribution is for tracks in which the microvertex detector (VD) participated in the track fit.

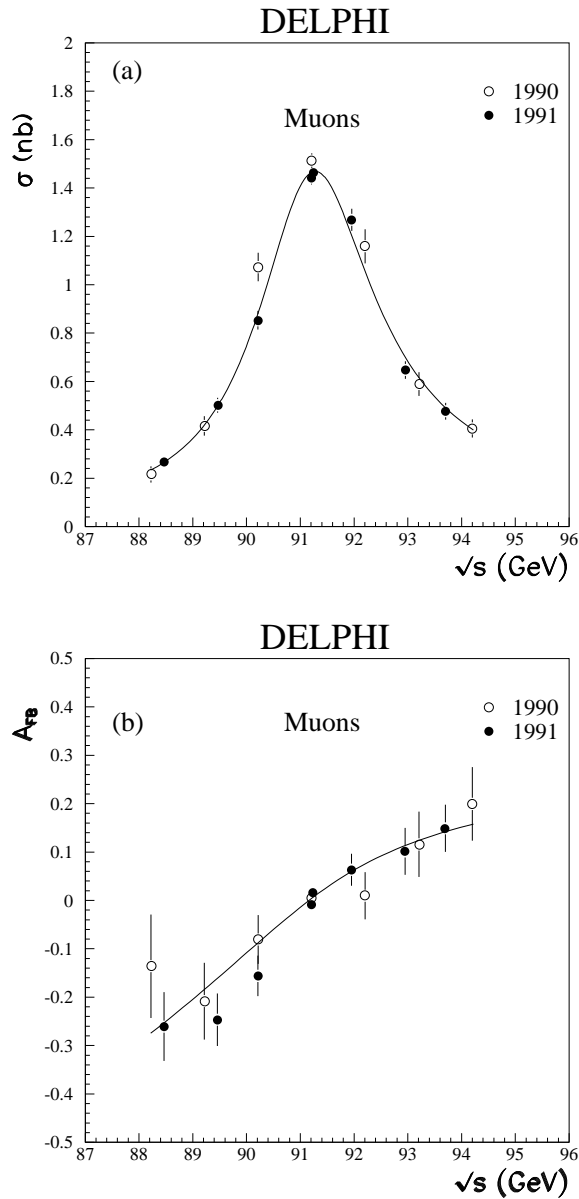


Figure 7: Cross sections and forward-backward charge asymmetries in the  $\mu^+\mu^-$  channel  
 (a) Cross sections extrapolated to the full solid angle and corrected for the acollinearity and momentum cuts.

(b) Forward-backward charge asymmetries by the likelihood method, extrapolated to the full angular range.

The curves are the results of the 5-parameter fit described in Section 7.

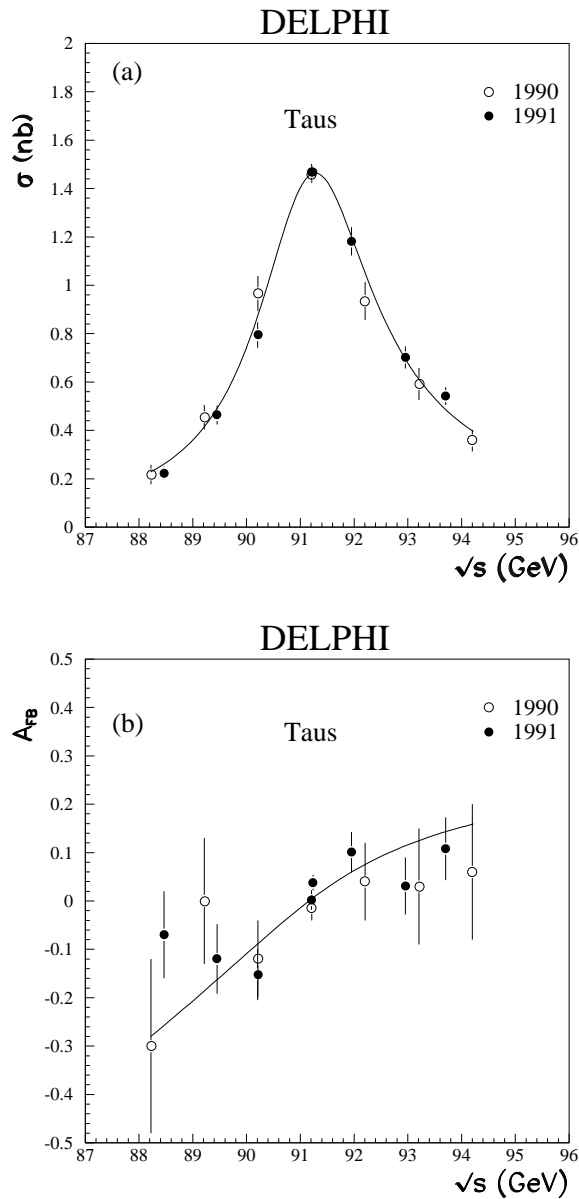


Figure 8: Cross sections and forward-backward charge asymmetries in the  $\tau^+\tau^-$  channel  
 (a) Cross sections extrapolated to the full solid angle and corrected for experimental cuts.  
 (b) Forward-backward charge asymmetries by the likelihood method, extrapolated to the full angular range.

The curves are the results of the 5-parameter fit described in Section 7.

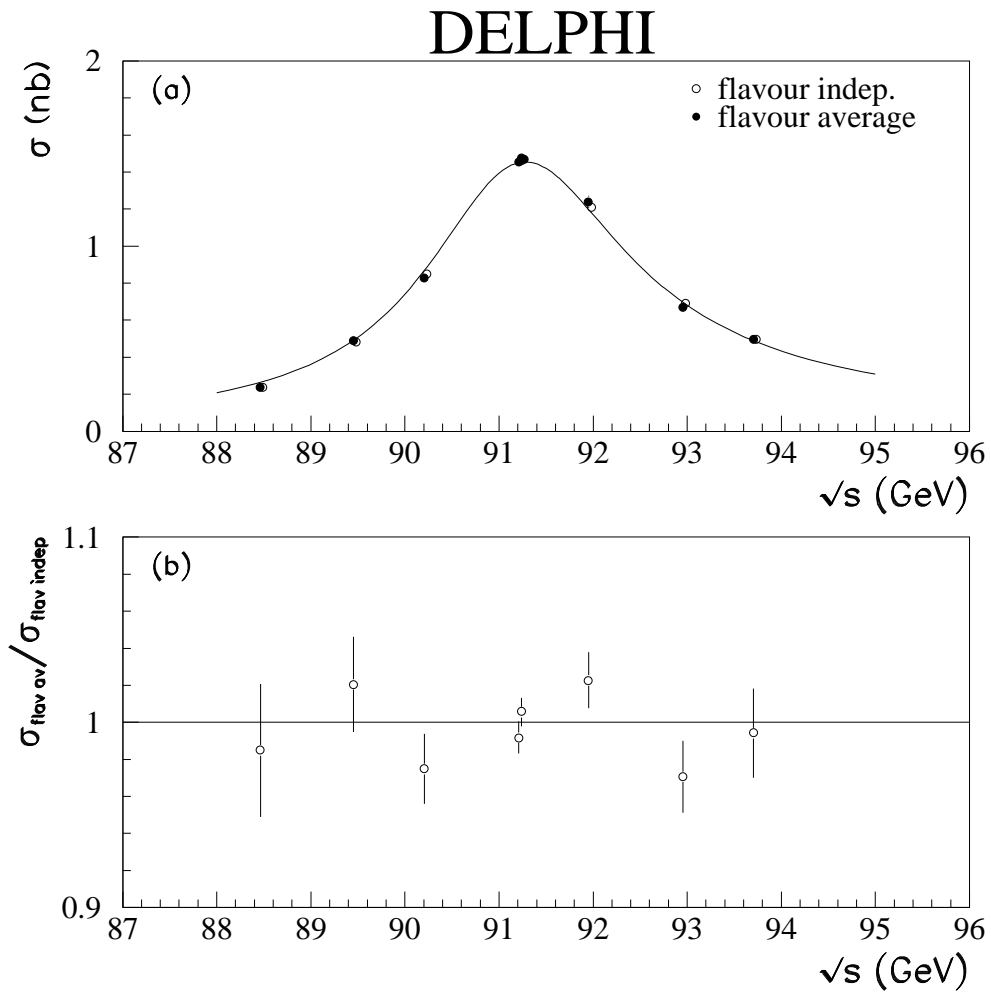


Figure 9: The cross sections for the lepton flavour independent and the weighted average of the lepton identified cross sections for the 1991 data, all corrected to  $4\pi$  acceptance, are shown in (a) as a function of the centre-of-mass energy. The errors are statistical only, and the flavour independent points are shifted slightly in energy for clarity. The curve is the result of the 5-parameter fit described in Section 7. In (b) are shown the ratios of these cross sections, with errors taking into account both the systematic errors and the statistical correlation between the samples.



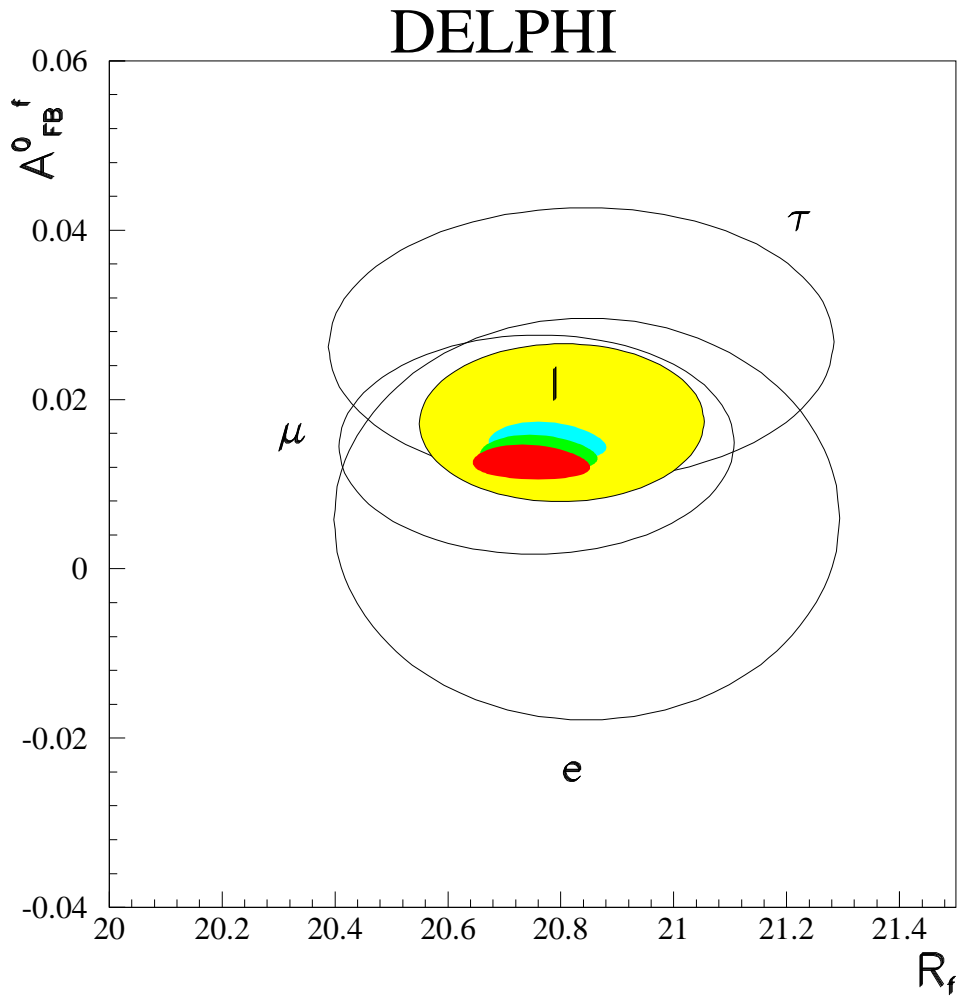


Figure 10: Allowed contours in the  $A_{\text{FB}}^{0f} - R_f$  plane. The contours from the 9-parameter fit, without assuming lepton universality, are indicated by  $e$ ,  $\mu$  and  $\tau$ , while the region allowed by the 5-parameter fit assuming lepton universality is indicated by  $l$  and is lightly shaded. The contours represent 68% confidence limits. The smaller shaded areas show the predictions of the Standard Model for  $m_t = 140 \pm 30$  GeV and  $\alpha_s = 0.12 \pm 0.01$  and for Higgs masses of 60 GeV (lightest shading), 300 GeV and 1000 GeV (darkest shading).

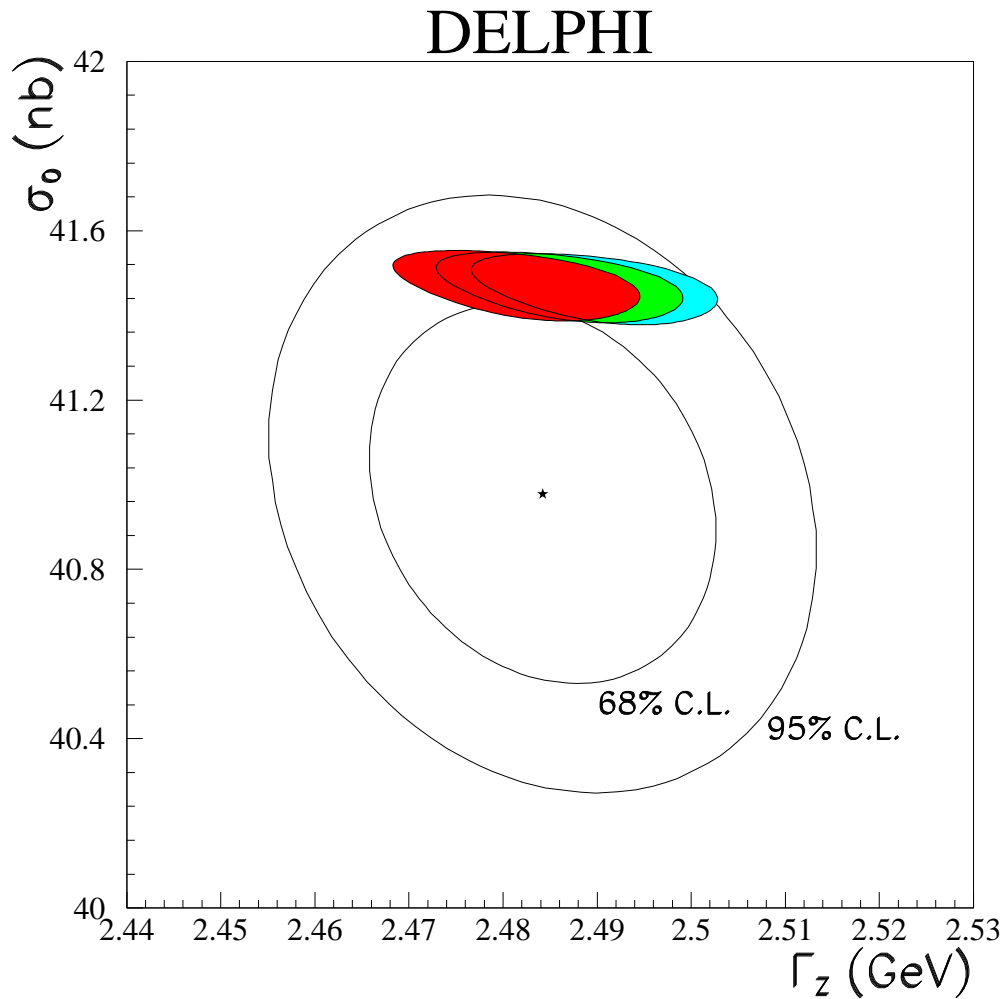


Figure 11: Allowed contours in the  $\sigma_0 - \Gamma_Z$  plane, from the 5-parameter fit assuming lepton universality. The contours represent 68% and 95% confidence limits. The shaded areas show the predictions of the Standard Model for  $m_t = 140 \pm 30$  GeV and  $\alpha_s = 0.12 \pm 0.01$  and for Higgs masses of 60 GeV (lightest shading), 300 GeV and 1000 GeV (darkest shading).

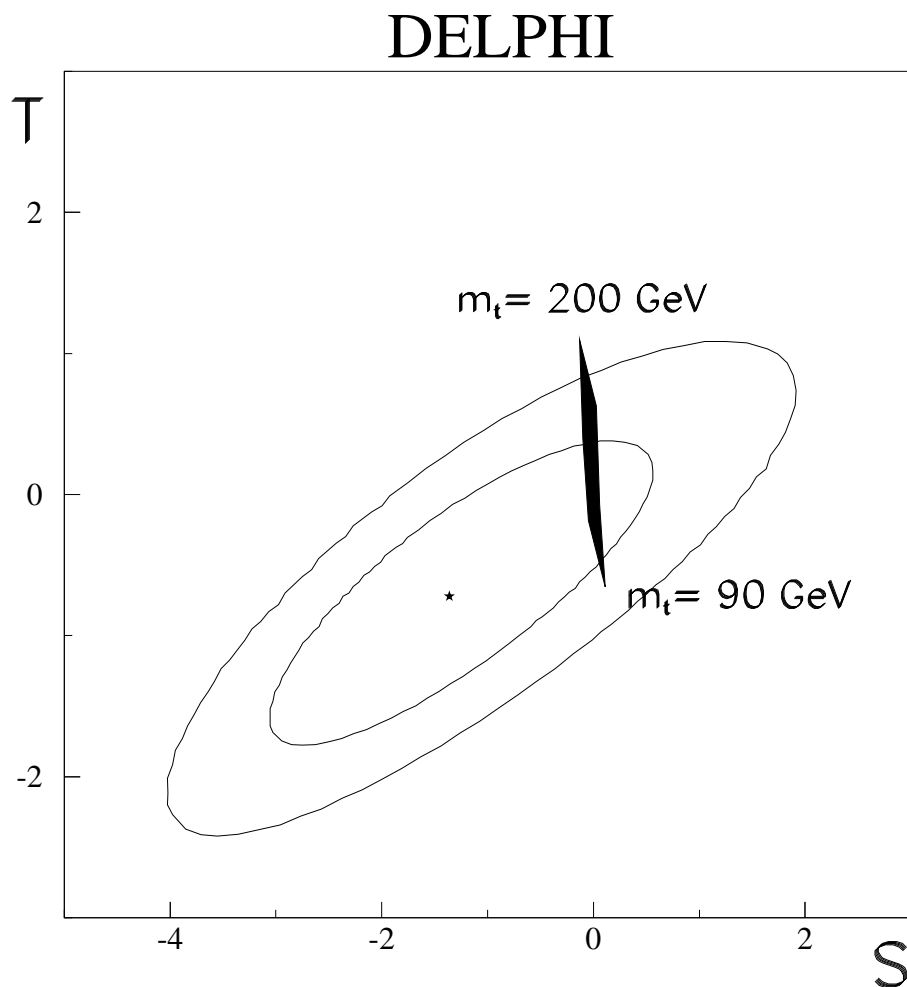


Figure 12: A fit of the variables S and T to the 1990 and 1991 data. The contours show the 68% and 95% confidence limits. The black area shows the predictions of the Minimal Standard Model for a range of top quark masses, and for Higgs masses in the range 50 GeV to 1000 GeV